AD-A071 023 GTE LABS INC WALTHAM MASS F/G 20/5
NEW LASERS BASED ON TRANSITION METAL COMPLEXES.(U)
APR 79 L ANDREWS, E JOHNSON, A LEMPICKI F49620-77-C-0015
UNCLASSIFIED TR-79-740.1 AFOSR-TR-79-0832 NL

END
DATE FILMED
8-79
DDC

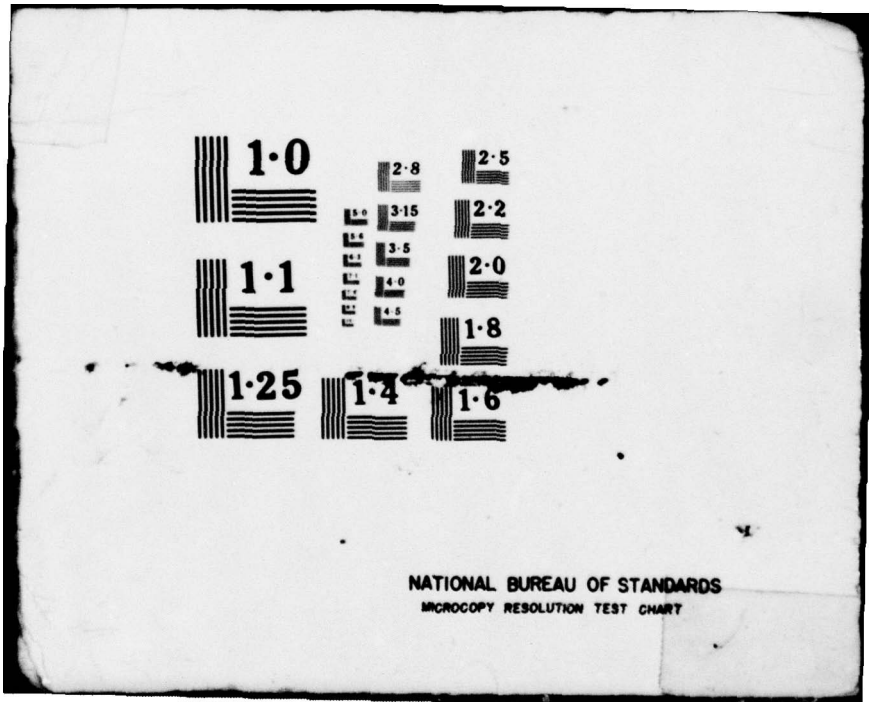
1·0
1·1
1·25
1·4
1·6
1·8
2·0
2·2
2·5
2·8
3·15
3·5
4·0
4·5
NATIONAL BUREAU OF STANDARDS
MICROCOPY RESOLUTION TEST CHART

TR 79-740.1

NEW LASERS BASED ON TRANSITION METAL COMPLEXES

by

L. Andrews
E. Johnson
A. Lempicki

Contract No. F49620-77-C-0015

FINAL REPORT

October 1, 1976 through October 1, 1978

AIR FORCE OFFICE OF SCIENTIFIC RESEARCH
Bolling Air Force Base
Washington, D.C. 20332

April 1979

GTE LABORATORIES INCORPORATED
40 Sylvan Road
Waltham, Massachusetts 02154

TABLE OF CONTENTS

Section		Page
1	Introduction	1
2	Structure and Spectroscopy of TM Complexes	2
	2.1 Ruthenium(II)	4
	2.2 Iridium(III)	8
	2.3 Iridium(I) and Rhodium(I)	9
	2.4 Rhenium(I)	11
	2.5 Octaethylporphyrin	12
3	Flashlamp Pump Experiments	13
	3.1 Active Medium and Resonator	13
	3.2 Flashlamp Pumps	14
	3.3 Laser Experiments	16
4	TM Complex Laser Experiments Using a Doubled Nd-Glass Pump	19
	4.1 Introduction	19
	4.2 Experimental Setup	19
	4.3 Resonator Analysis	22
	4.4 Application of Analysis to Experimental Situation	34
	4.5 Experimental Results	36
	4.6 Discussion	36
5	Conclusions	39
6	References	43
Appendix		
A-1	Excitation Polarization of Luminescent Iridium(I) and Rhodium(I) Phosphine Complexes	A-1
B-1	Radiationless Decay in Rhodium(I) and Iridium(I) Complexes: Polarization and Solvent Relaxation Studies	B-1

LIST OF ILLUSTRATIONS

Figure		Page
1	Absorption and Emission of $Ru(bipy)_3Cl_2$	6
2	Rates of Excitation for $Ru(bipy)_3Cl_2$	7
3	Absorption and Emission of $Rh(P=P)_2Cl$	10
4	Rates of Excitation for $Rh(P=P)_2Cl$	11
5	Construction of Piston Cell	14
6	Circuit for the 400J Flashlamp Pump	15
7	Emission Profile of $Ru(\phi_2\ phen)_3Cl_2$ Pumped at 1000J	17
8	Block Diagram of Experimental Setup	19
9	Photograph of Experimental Setup	20
10	Photograph of Resonator	21
11	Schematic Diagram of Resonator	21
12	Resonator Model for Calculations	25
13	Delay Before Onset of Lasing	30
14	Pulsed Thresholds	31
15	Time Dependence of Gain for Various Ranges of Excited State Lifetime	33
16	Simplified Energy Level Diagram Appropriate for Modules Containing First Row Atoms	40

1. INTRODUCTION

The purpose of this program has been to investigate the possibily that luminescent transition metal complexes (TM complexes) might serve as the basis for a new class of lasers tunable in the visible spectral region. At the beginning of the program, sufficient spectroscopic and photophysical data were available to permit calculation of threshold requirements for these new materials, and they were found to lie well within the range of conventional pump sources. This threshold analysis assumed perforce that losses which are unknown do not exist. In particular, data concerning losses due to excited-state absorption at the luminescence wavelengths are either incomplete or nonexistent for these materials.[1-5] This state of affairs is hardly surprising in view of the complexity of excited-state absorption measurements. In fact, little data is available on the excited-state absorption of fluorescent organic dyes which have been otherwise extensively studied.[6-8] Rather than attempt to fill this gap in the spectroscopy of TM complexes, the decision was made to proceed with laser experiments after synthesizing the complexes and carrying out preliminary screening with low-energy pulsed excitation.

Virtually, none of these materials is commercially available, so that a large portion of the first year was devoted to synthesis and purification of complexes which appeared most promising for laser applications. This amounted to five groups of materials: metalloporphyrins; ruthenium (II), iridium (III) and rhenium (I) complexed with nitrogen heterocycles (d^6 systems); and square planar rhodium (I) and iridium (I) phosphines (d^8 systems). Emission spectra and lifetimes were routinely measured and compared with literature data to positively identify all synthesized complexes.

The first pulsed experiments were done at a low energy (20J) with a xenon flashlamp and were designed to compare the peak fluorescence intensity of a known laser dye with the peak emission of TM complexes. Such peak-intensity ratios are complex functions of radiative lifetimes, absorption spectra, concentrations, and excitation spectral distribution and intensity. Without performing a detailed analysis incorporating all of these variables, it was possible to infer from the observed peak intensity ratios that thresholds for TM complexes should be within the reach of conventional pump sources, a conclusion which confirmed the calculated thresholds. This observation is a necessary but not sufficient condition for lasing.

Toward the end of the first year, a 400J xenon flashlamp apparatus was completed and preliminary laser experiments were attempted. These continued into the second year while construction of a second generation 1200J xenon flashlamp apparatus was completed. All promising complexes were subsequently tested with the higher energy pump. In addition, a frequency doubled, Q-switched Nd:glass laser was assembled and used to pump complexes in specially designed low-loss resonators. Only Ru(II) and metalloporphyrins were tested with this multimegawatt laser as these are the only materials with pump bands appropriate for 5300Å radiation. Under no conditions was laser action detected from any luminescent TM complex.

The sections which follow contain an overview of the electronic spectroscopy of TM complexes and a complete list of complexes which were synthesized and evaluated during the program. A discussion of specific properties of each group of complexes was given in the Annual Report. This has been augmented and for completeness sake is included here. This is followed by a detailed description of the flashlamp pump apparatus and the laser pump apparatus together with a description of the resonators used in the laser pump experiments. An analysis is also given of the effect of pump pulse duration on threshold requirements. Finally, a concluding section presents a rationale for the absence of laser action in TM complexes and a strong recommendation is given for carrying out appropriate excited state absorption measurements to settle the issue of whether laser action can ever be achieved at any pump level in this group of luminescent materials.

2. STRUCTURE AND SPECTROSCOPY OF TM COMPLEXES

In general, luminescent TM complexes incorporate a second or third row transition metal ion bound to an organic ligand such as 1,10-phenanthroline or a porphyrin derivative. Numerous spectroscopic investigations have established that the resulting molecular electronic transitions which are of interest in laser applications may be classified as either ligand localized (π, π^*) or metal ligand charge transfer.[9] Absorptions are frequently intense and are found throughout the visible spectral region.

Emission occurs only from the lowest excited electronic state (or from states thermally accessible from the lowest state) and is always partially forbidden. It is this forbiddenness which distinguishes the luminescence of TM complexes from the fluorescence characteristic of purely organic materials and raises the possibility of energy storage and Q-switched operation. The origin of this forbiddenness may be understood by the following qualitative description. Electronic transitions in molecules comprised of light atoms may be classified as spin forbidden or spin allowed. In the usual case, this given rise to a singlet manifold of states optically accessible from the ground state and a triplet manifold accessible only indirectly via intersystem crossing from the singlet levels. The introduction of a heavy metal ion into the molecule blurs the spin distinction since levels become mixed due to spin-orbit coupling and spin labels are no longer appropriate. Nevertheless, the distinction is not completely lost as evidence by the relatively long radiative lifetimes found in TM complexes. In fully allowed transitions, lifetimes are measured in nanoseconds, whereas in highly forbidden transitions, excited states may persist for seconds. TM complex emissions lie in the range 10^{-4}s to 10^{-5}s, between the extremes, and may be considered highly perturbed levels of triplet origin. This opens the possibility of high-powered devices pumped with microsecond flashlamps.

A second consequence of strong spin orbit coupling is a very rapid conversion of upper levels to the emitting level. Luminescence is never observed from upper levels not in thermal equilibrium with the lowest level. This is in contrast to organic dyes in which fluorescence is commonly seen to compete effectively with conversion to the lowest electronically excited level (the lowest triplet). This relaxes the requirements somewhat for the risetime of the pump pulse in that it need not be fast compared with an intersystem crossing rate which populates an optically metastable lowest level. In TM complexes, it is the lowest level which is of interest, and

any excited state absorption losses associated with this level are independent of the rate at which it is populated. The analogous losses in organic dye lasers are singlet-singlet absorption from the fluorescent level. We will comment further on these points in the Conclusion Section.

2.1 RUTHENIUM(II)

Hexacoordinate Ru(II) complexes containing the bidentate ligands 1,10-phenanthroline (phen) and 2,2'-bipyridine (bipy)

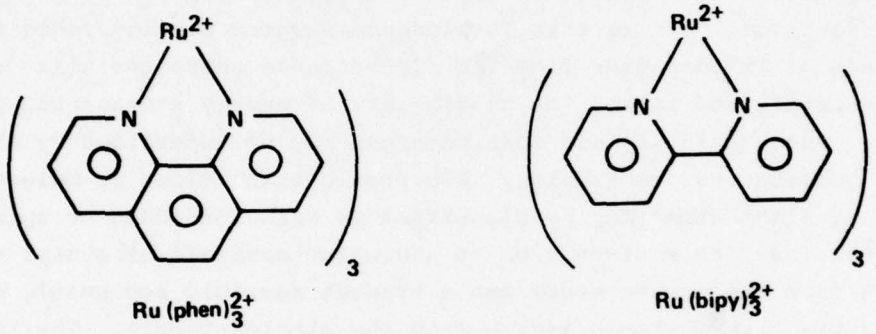

were among the earliest discovered highly luminescent complexes and are the most well studied.[9] A number of derivatives have been synthesized which incorporate phenyl, methyl and halogen substituents in the ligand rings.

These complexes emit in the region 0.55 μm to 0.75 μm and have emission lifetimes in the range 4 μs to 10 μs in alcoholic hosts at the temperature of liquid nitrogen. At room temperature, emission intensities are appreciable in fluid solution and are enhanced by incorporating the complexes in rigid plastic hosts such as polymethylmethacrylate and polyesters. Even in plastics, the room-temperature lifetimes are at least a factor of two less than the lifetimes at liquid-nitrogen temperature.

Low energy (20J) flash experiments show that the peak luminescence intensities are factors of 20 to 40 less than the peak fluorescence intensity of a 10^{-3}M Rhodamine-6G dye solution. This means that Ru(II) complexes, will have threshold pump-power requirements at least a factor of 20 to 40 greater than Rhodamine-6G. Although this estimate is only a necessary and not sufficient requirement for lasing, it does indicate that laser action is a possibility with conventional flashlamp pumping.

For a four-level system, the minimum population of the upper laser level necessary to achieve threshold is given by:[11]

$$\Delta n \geq 4\pi \, \Delta\lambda \, \tau_R / \lambda^4 t_c$$

where:

λ is the emission maximum,

$\Delta\lambda$ is the emission bandwidth at half height,

τ_R is the radiative lifetime,

t_c is the cavity lifetime.

Using parameters appropriate for $Ru(bipy)_3Cl_2$ in 1-propanol at -150°C, we have:

$$\tau_R = 1 \times 10^{-5} s$$

$$t_c = 1 \times 10^{-9} s$$

$$\lambda = 600 \text{ nm}$$

$$\Delta\lambda = 80 \text{ nm}$$

$$\Delta n \geq 1.3 \times 10^{-4} \text{ moles } \ell^{-1}$$

Absorption spectra and the emission spectrum of $Ru(bipy)_3Cl_2$ under these conditions are shown in Figure 1. At the concentrations which are necessary for laser action ($>10^{-4}$ moles ℓ^{-1}), Figure 1 shows that ground-state absorption losses are significant at wavelengths shorter than 610 nm but that lasing is a possibility at longer wavelengths. This is a common occurrence in fluorescent organic dyes in which ground-state absorption losses limit laser oscillation to the red edge of the fluorescence band. At present, the data are lacking to assess luminescent-state absorption losses. Only one study[5] has appeared on the excited state absorption of $Ru(bipy)_3Cl_2$ and this was confined to wavelengths shorter than 500 nm, although at 500 nm this absorption was very weak if present at all.

At high concentrations, Ru(II) complexes exhibit intense absorption in the visible which leads to highly nonuniform optical pumping. In a cylindrical cell, it is expected that the modes with the lowest thresholds will be at the center of the cell, so it is important to adjust the complex concentration and cell size to permit a large rate of excitation at a

pentration depth equal to the cell radius. The total rate of excitation R over the entire absorption band $\Delta\lambda$ at a depth x is given by:[11]

$$R(x) = \int_{\Delta\lambda} P^{O}(\lambda) \quad \phi(\lambda) \; \alpha(\lambda) \; \exp[-a(\lambda)x] \, d\lambda$$

where:

$P^{O}(\lambda)$ is the number of pump photons per cm^2/s

$\phi(\lambda)$ is the luminescent quantum efficiency,

$\alpha(\lambda)$ is the absorption constant.

In the approximation that $P^{O}(\lambda)$ and $\phi(\lambda)$ are constant, the rate of excitation is proportional to:

$$K = \int_{\Delta\lambda} \alpha \exp[-\alpha x] \, d\lambda$$

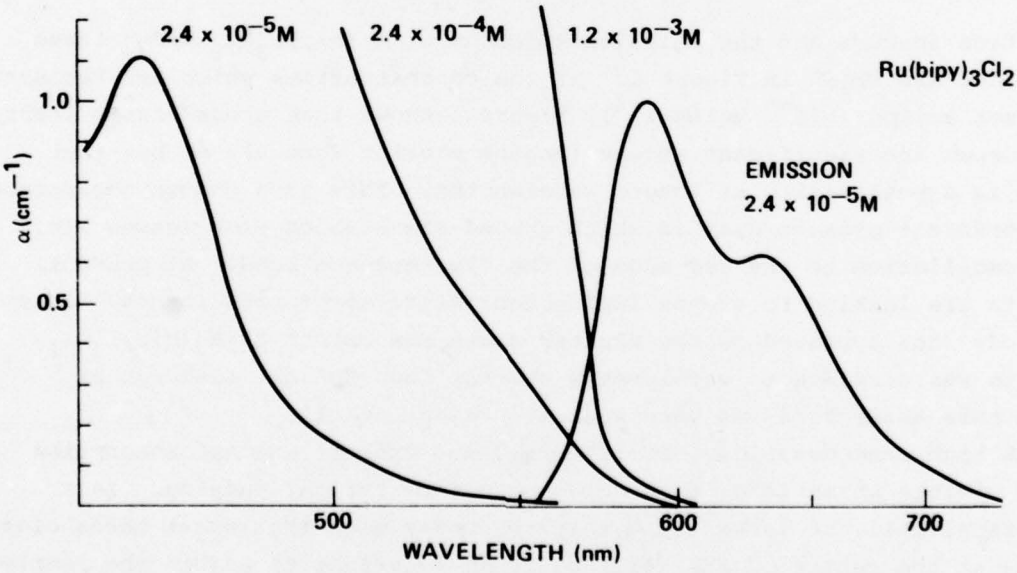

Figure 1. Absorption and Emission Spectra of $Ru(bipy)_3Cl_2$ in 1-Propanol at -150°C

In Figure 2, the function $\alpha \exp[-\alpha x]$ is computed at the cell radius for 5×10^{-4} moles ℓ^{-1} $Ru(bipy)_3Cl$ in 1-propanol at -150°C for 1 mm, 2.5 mm and 5.0 mm diameter cells. Integration between 400 nm and 570 nm leads to pump excitation rates of 11, 33 and 68 $\times 10^{-6}$, respectively. These rates compare quite favorably with ruby and europium chelate lasers[11] and show that Ru(II) complexes can be effectively pumped.

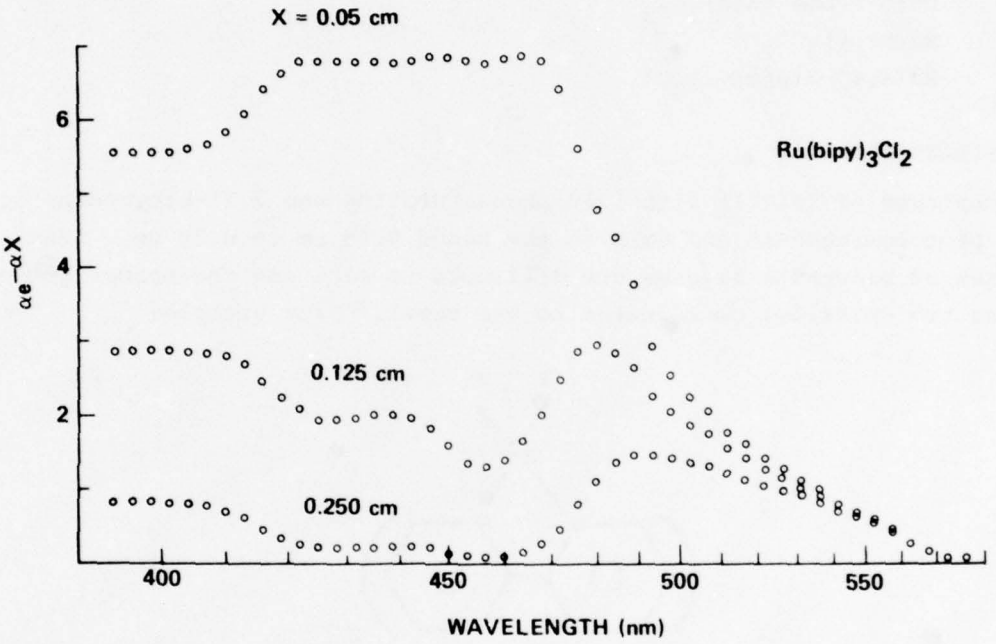

Figure 2. Rates of Excitation for $Ru(bipy)_3Cl_2$ in 1-Propanol at -150°C Calculated at the Center of 0.1 cm, 0.25 cm and 0.5 cm Diameter Laser Cells

The complex $Ru(bipy)_3Cl_2$ is typical of this group of materials. Substitution of phenyl or methyl groups causes small red shifts in absorption or emission spectra as well as intensification of absorption by about a factor of two. Similar remarks apply to replacement of bipyridine ligands with phenantholine, and room temperature as well as liquid nitrogen temperature spectra and photophysical properties have been summarized for a variety of these complexes.

Ru (II) Complexes Synthesized:

$Ru(phen)_3Cl_2$
$Ru(4,7\text{-diphenyl phen})_3Cl_2$
$Ru(4,7\text{-dimethyl phen})_3,Cl$
$Ru(3,4,7,8\text{-tetramethyl phen})_3Cl_2$
$Ru(2,9\text{-dimethyl-}4,7\text{-diphenyl phen})_3Cl_2$
$Ru(5,6\text{-dimethyl phen})_3Cl_2$
$Ru(5\text{-bromo phen})_3Cl_2$
$Ru(bipy)_3Cl_2$
$Ru(4,4'\text{-diphenyl})_3Cl_2$

2.2 IRIDIUM(III)

Complexes of Ir(III) with 1,10-phenanthroline and 2,2'-bipyridine are highly photoluminescent and emit in the range 0.45 μm to 0.70 μm. Tris complexes of bidentate ligands are difficult to make and the normal product contains two chlorides coordinated to the metal,[12] for example:

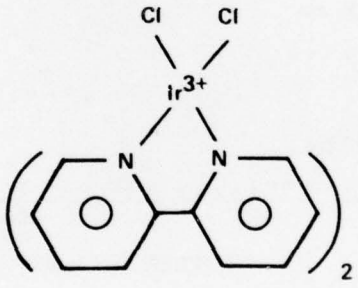

$Ir(Cl_2\ bipy_2)^+$

Unlike Ru(II), variations in ligands (bipy, phen and their derivatives) can cause major changes in the photophysical properties of Ir(III) complexes. This has been explained by invoking two electronically excited states, one a metal to ligand charge transfer (MLCT) state and the other a ligand centered π, π^* state, which are energetically very close.[13] Minor changes in chemical structure or solvent can cause one or the other to be lower in energy and therefore to be the emissive state. For laser applications, it is the MLCT state, as it is in Ru(II) complexes, which is of interest and complexes which show MLCT emission have lifetimes and yeilds very similar to Ru(II) complexes.

Low-energy peak-intensity measurements show Ir(III) complexes to be a factor of four less intense than Ru(II) complexes. This is very likely due to less favorable pump bands which begin near 450 nm and rise sharply to high values for α. A more serious drawback, however, is the photo-labelization of the chloride ligands which are irreversibly lost during illumination in fluid solution.[14] This behavior is not limited to the dichloro complexes, as the tris complex $Ir(bipy)_3Cl_3$[15] also shows photo-degradation. Although this chemistry may ultimately limit the utility of Ir(III) complexes, it probably is not a problem in low temperature glasses, and should not affect single shot laser experiments.

Ir(III) complexes synthesized:

$Ir(Cl_2\ phen_2)Cl$
$Ir(Cl_2\ bipy_2)Cl$
$Ir(Cl_2$ (4,7-diphenyl phen)$_2)Cl$
$Ir(Cl_2$ (4,4'-diphenyl bipy)$_2)Cl$

2.3 IRIDIUM(I) AND RHODIUM(I)

Recently, it has been reported that square planar complexes of Ir(I) and Rh(I) with the diphosphine ligand cis-1,2-(diphenylphosphino)ethylene (P=P) are luminescent.[16]

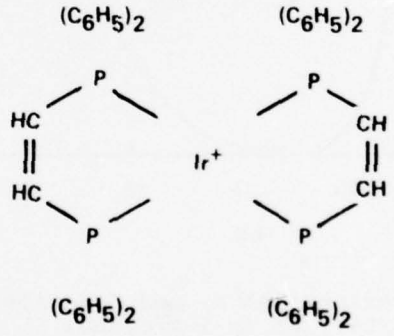

$Ir(P{=}P)_2^+$

In alcoholic solution at -190°C, $Ir(P{=}P)_2Cl$ has a 9.4 μs emission lifetime and shows a narrow emission band centered at 546 nm. It has effective pump bands between 400 nm and 550 nm; however, the Stokes shift is small and there is extensive overlap between absorption and emission which leads to

serious losses. The only hope of achieving stimulated emission under these conditions is to have substantial depopulation of the ground state. Because the emission bandwidth is small ($\Delta\lambda \approx 15$ nm), the minimum population required for oscillation is $\Delta n \geq 3 \times 10^{-5}$ moles ℓ^{-1} and complete conversion is a possibility. Nevertheless, it is doubtful that this complex can be of practical importance as a laser because it irreversibly reacts with oxygen to yield a nonluminescent O_2-adduct. $Rh(P{=}P)_2Cl$ has a 29.5 μs emission lifetime at -165°C and shows broad emission (λ = 595 nm, $\Delta\lambda$ = 70 nm). Unlike the Ir(I) analog, $Rh(P{=}P)_2Cl$ emission has a very large Stokes shift and consquently negligible losses due to ground state absorption.

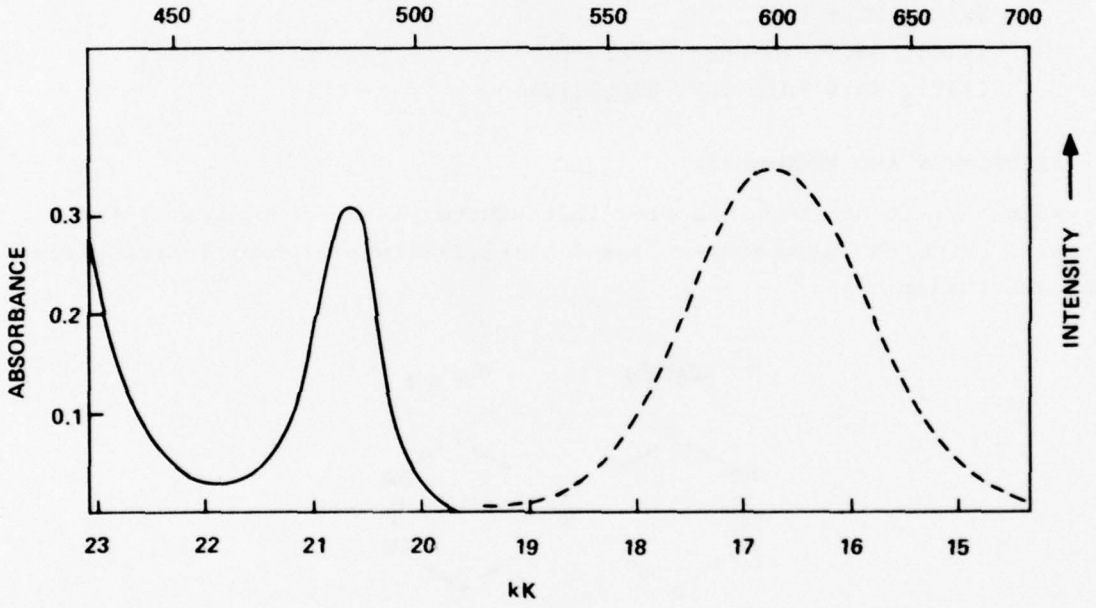

Figure 3. Absorption (137°K) and Emission (94°K) Spectra of $Rh(P{=}P)_2Cl$ in 1-Propanol

Furthermore, this complex has effective pump bands between 400 nm and 500 nm at high concentration.

The spectroscopy and photophysics of these diphosphine complexes were investigated in detail and full reports are included in the appendixes. We only note here that neither complex emits in fluid solution and that this is due principally to a viscosity dependent nonradiative decay path.

Complexes synthesized:

$Ir(P{=}P)_2Cl$
$Ir(P\text{-}P)_2Cl$
$Rh(P{=}P)_2Cl$
$Rh(P\text{-}P)_2Cl$

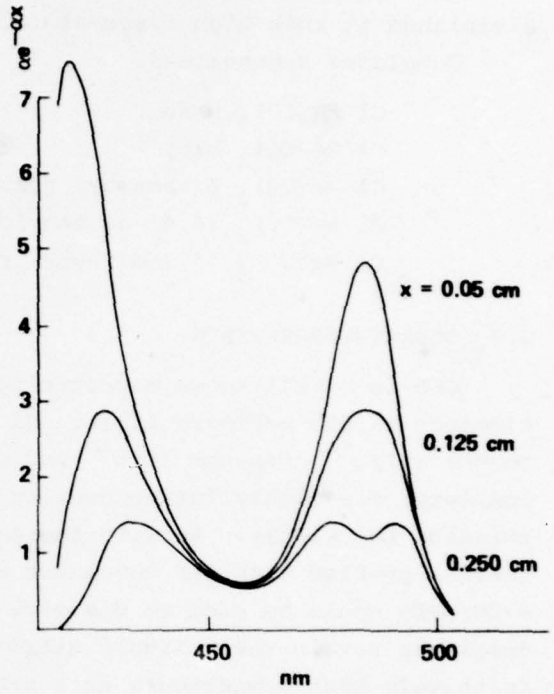

Figure 4. Rates of Excitation for $Rh(P{=}P)_2Cl$ at 2×10^{-3}M in 1-Propanol for Cylindrical Cells with Radius 0.05, 0.125 and 0.25 cm

2.4 RHENIUM(I)

Another class of recently discovered luminescent complexes are tricarbonylchloro Re(I) X, where X can be a wide variety of mono and bidentate nitrogen containing ligands.[17]

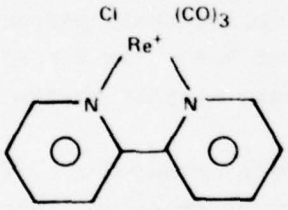

Cl $Re(CO)_3$ bipy

Although the properties of these complexes have not been extensively investigated, they appear to have MLCT emissive states with liquid nitrogen lifetimes in the range 1 μs to 10 μs. Many emit weakly at room temperature in fluid solution, and some, the phen and bipy derivatives, appear to have substantial emission yields at liquid N_2 temperatures. A limiting feature of these materials is their low solubility in common solvents. We have found, however, the ϕ_2 phen derivative to be quite soluble in α-chloronaphthalene/methylethylphthylglycolate(1/1)* which forms a stable glass at

*Referred to as α-Cn/MPEG

210°K. Unfortunately, the emission yield of this complex is somewhat diminished at this high temperature.

Complexes synthesized:

Cl $Re(CO)_3$ phen
Cl $Re(CO)_3$ bipy
Cl $Re(CO)_3$ (3-benzoyl pyridine)$_2$
Cl $Re(CO)_3$ (4,4'-diphenyl bipy)
Cl $Re(CO)_3$ (4,7-diphenyl phen)

2.5 OCTAETHYLPORPHYRIN

OEP is a well-known macrocyclic ligand which will coordinate most elements in the periodic table. Of interest for laser applications are the copper (II),[18] platinum (II)[19] and palladium (II)[20] complexes. These complexes are highly luminescent at low temperatures and show narrow emission bandwidths. As with the previously described Re(I) complexes, a serious problem with OEP complexes are their low solubilities. Again, 1/1 α-CN/MPEG could be used to dissolve up to 10^{-2} moles ℓ^{-1}. Furthermore, OEP complexes retain their liquid nitrogen photophysical properties at relatively high temperature in a α-CN/MPEG. For example, at -20°C, Pt OEP has a 120 μs emission lifetime and a bandwidth of 11.2 nm (λ = 644) virtually identical to its properties at -196°C. Using these parameters and the reported luminescence quantum efficiency of 0.9,[11] Δn for Pt OEP is calculated to be 2×10^{-4} moles ℓ^{-1} which is very similar to the value for Ru(II) complexes.

The absorption constant for Pt OEP has not been measured in α-CN/MPEG at -20°C, but the room temperature value in methylene chloride indicates that the window between 400 nm and 500 nm in the absorption spectrum can be effectively pumped (α = 8 cm^{-1} at 10^{-3} moles ℓ^{-1} at 450 nm).

Complexes synthesized:

Cu OEP
Pd OEP
Pt OEP

3. FLASHLAMP PUMP EXPERIMENTS

It is clear that for TM complexes to have practical utility as lasers, they must be susceptible to pumping by incoherent sources, specifically flashlamps. Accordingly, two flashlamp pumps were constructed during this program; a single lamp apparatus capable of 400J input energy and a double lamp apparatus capable of 1200J. These were used to screen all classes of materials for laser action.

3.1 ACTIVE MEDIUM AND RESONATOR

By far the most convenient method for handling the TM complexes for laser experiments is in a solution of an organic solvent which forms a stable, optically clear glass at low temperatures. A number of solvents and solvent mixtures are known to form glasses,[21] and the specific choices used here were dictated by TM-complex solubility. Ru(II) and Ir(III) complexes dissolve readily in 1-propanol and with careful temperature control, this alcohol forms a clear glass at 110°K, although severe cracking does occur below 105°K. Ir(I) or Rh(I) material was dissolved in 1-propanol or a 4/1 mixture of methanal/ethanol. Slightly lower temperatures could be achieved with the mixed alcohol solvent and this was considered worthwhile because of a temperature-dependent radiationless decay process discovered in the Ir(I) complex (Appendix 2). The OEP and Re(I) complexes could only be dissolved to high concentrations in α-CN/MPEG which can be cooled to 210°K. In all of these systems, concentrations up to 10^{-2} moles ℓ^{-1} could be achieved.

In order to take advantage of the glass-forming properties of these solvents, it was necessary to design a laser cavity which could accommodate solvent contraction, usually a 20% decrease in volume, while maintaining a high degree of optical perfection within the resonator. This problem was solved in an earlier study of liquid lasers by using a quartz piston cell[22] and such a design was adopted here. In this scheme, a precision bore quartz tube is fitted with quartz pistons approximately 2 cm in length which are ground so as to just permit free movement within the tube. The spacings between the pistons and the inner wall of the tube is small enough so that the solvent surface tension effectively prevents liquid flowing out of the assembled cell. As the cell is cooled, solvent contraction pulls the pistons into the quartz tube during which contact is maintained between the pistons and the solution. Eventually

the solvent viscosity becomes sufficiently high to freeze the pistons in place, and further cooling causes bubble formation. The ends of the pistons in contact with solution are ground with a large radius of curvature (~1M) and coated with broadband hard dielectric mirrors. One set of pistons had fully reflective mirrors (99.8%) over the range 4500 to 7000Å and another set were partial reflectors (97 ± 2%) over the same range. Two piston cells were used which were 7 cm long and had either 5 mm or 1 mm bores about 4 cm long (Figure 5).

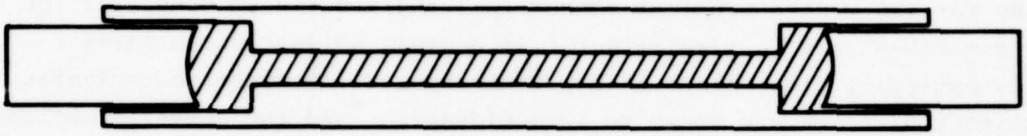

Figure 5. Construction of Piston Cell. TM complex solution is shown as shaded area and the radius of curvation of the pistons is exagerated.

The same pistons could be used in either cell. Also, the 5 mm bore cell could be fitted with inserts reducing the diameter to 2.5 mm or 1 mm.

Sample Preparation Procedure

An appropriate amount of TM complex was accurately weighed and dissolved in 5 cc of solvent. The solution was saturated with N_2 by bubbling for 10 min. During this time solvent loss by evaporation was negligible. The solution was then stoppered and transferred to a glove bag previously flushed with N_2. The solution was poured into a syringe fitted with a Millipore filter holder and passed through a 0.5μ Tefion filter (Millipore FHLP 01300) directly into the piston cell which was then assembled within the glove bag. The cell was removed and immediately placed in the flashlamp pump apparatus dewar which was thoroughly flushed with cooled N_2.

3.2 FLASHLAMP PUMPS

The 400J apparatus used a single flashlamp with a 5 or 7 mm diameter bore (Xenon, N-860C-5 or 7). It was fired using the overvoltage technique through a spark gap (EG&G GP-87) from a 2 μF, 25 kV, low inductance capacitor (Condensor Products CP205-30MXX). The pulse risetime was 1 to 2 μs with a half-power width of 10 to 15 μs. At the highest discharge

energies employed (400J), ringing could be detected in the lamp discharge indicating that a better match to the N-860C lamp resistance would have been obtained with a higher value capacitor discharged at a lower voltage to obtain the same input energy. This refinement, however, would have only marginally improved the lamp output during the first 5 μs, consequently, it was not incorporated into the pump. The spark gap trigger circuit shown in Figure 6 is of standard design and performed reliably. The flashlamp and dewar were optically coupled with a 22.5 cm diameter aluminized glass sphere. Threshold values for rhodamine-6G with this configuration were 5 to 10J. The piston cell was cooled by flowing cold N_2 gas through the dewar and the cell temperature was monitored by an iron-constantan thermocouple attached to the outside of the cell.

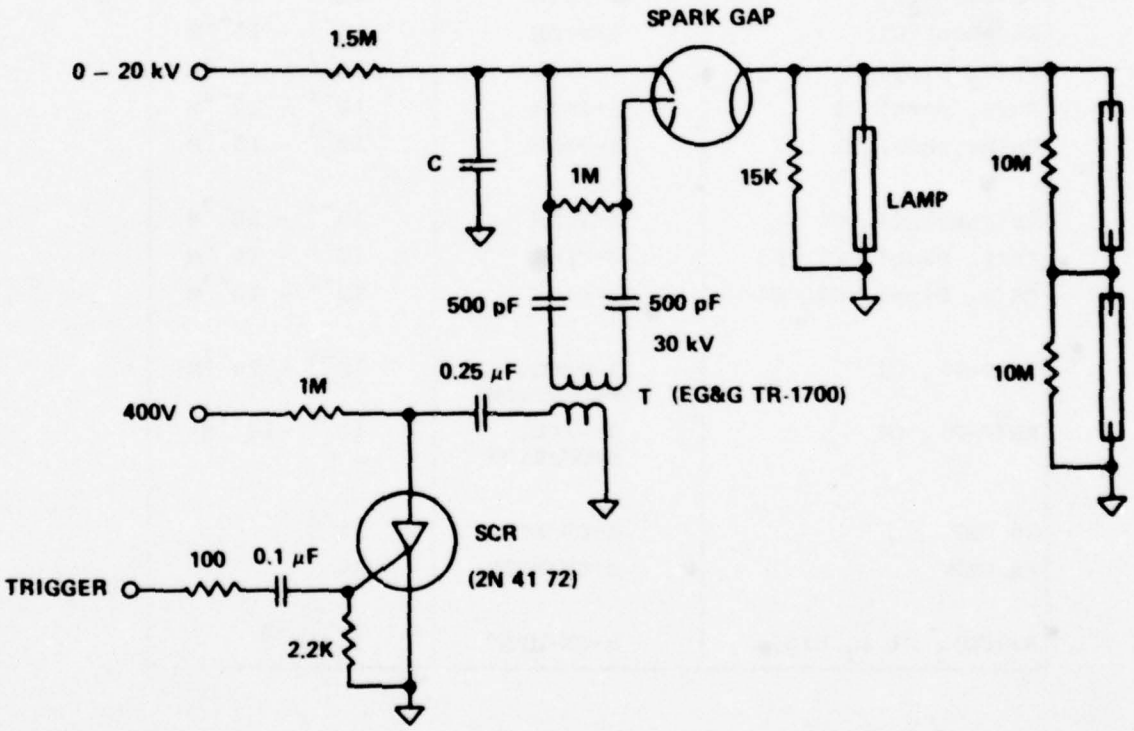

Figure 6. Circuit for the 400J Flashlamp Pump. The 1200J apparatus simply replaces the single lamp with the double lamp and parallel resistors. Value for C given in text.

The 1200J flashlamp pump used four low inductance capacitors (10 μF, 15 kV, Aerovox PX-75 D16) and two lamps (Xenon N860-5-100) connected in series (Figure 6). The spark gap was changed to EG&G Model GC-86 to ensure reliable firing at lower voltages. The pulse risetime was 5 μs with 25 μs half-power width. The lamps and dewar were coupled in a double elliptical, gold-coated enclosure (ellipse dimensions 5 × 7 cm) in which the dewar was aligned along the common focus.

3.3 LASER EXPERIMENTS

The following complexes were tested for laser action using the 400J and 1200J pumps.

COMPLEX	SOLVENT	CONCENTRATION
$Ru(bipy)_3Cl$	1-PrOH	10^{-3} - 10^{-2}M
$Ru(phen)_3Cl$	1-PrOH	10^{-3} - 10^{-2}M
$Ru(\phi_2\ bipy)_3Cl$	1-PrOH	10^{-3} - 10^{-2}M
$Ru(\phi_2\ phen)_3Cl$	1-PrOH	10^{-3} - 10^{-2}M
$Ru(Me_4phen)_3Cl$	1-PrOH	10^{-3} - 10^{-2}M
$Ir(phen)_2Cl_2\ Cl$	1-PrOH	10^{-3} - 10^{-2}M
$Ir(\phi_2\ phen)_2\ Cl_2\ Cl$	1-PrOH	10^{-3} - 10^{-2}M
$IR(\phi_2\ bipy)_2\ Cl_2\ Cl$	1-PrOH	10^{-3} - 10^{-2}M
$Ir(P{=}P)_2\ Cl$	1-PrOH, MeOH/EtOH	10^{-3} - 10^{-2}M
$Rh(P{=}P)_2\ Cl$	1-PrOH, MeOH/EtOH	10^{-3} -10^{-2}M
Cu OEP	α-CN/MPEG	10^{-2}
Pt OEP	α-CN/MPEG	10^{-2}
$Re(CO)_3\ Cl\ \phi_2\ bipy$	α-CN/MPEG	5×10^{-3}

Laser action was searched for with an RCA 7265 photomultiplier wired for fast-pulse applications. Typical data are shown in Figure 7 for $Ru(\phi\ phen)_3Cl_2$ in 1-propanol at 115°K. The shape of the emission pulse

closely follows the excitation pulse with no evidence of sharp structure which would signal lasing. Identical results were encountered for all complexes.

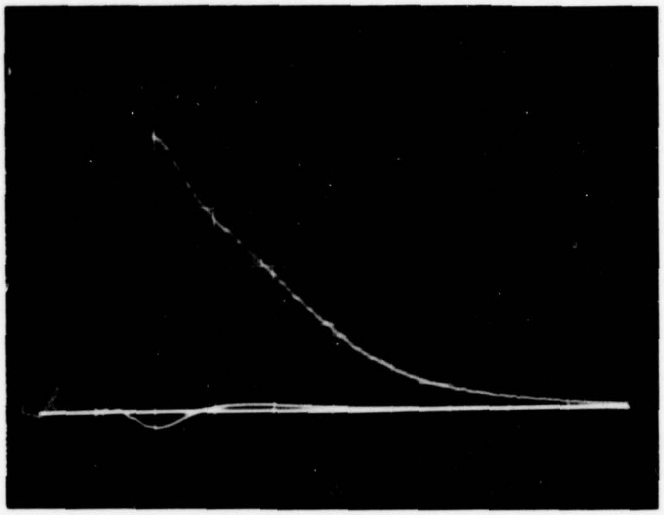

Figure 7. Emission Intensity of $Ru(\phi_2\ phen)_3Cl_2$ in Piston Cell Excited with 1000J Xenon Flashlamp Discharge.

4. TM COMPLEX LASER EXPERIMENTS USING A DOUBLED Nd-GLASS PUMP

4.1 INTRODUCTION

In investigating candidates for laser materials, pumping with a second laser has distinct advantages over flashlamp pumping. Absorption can be optimized over the entire bandwidth of the laser pump, and with good mode quality, tight focusing of the laser output can result in low thresholds. Further, the greater simplicity of the experimental setup lends itself better to estimates of thresholds.

To test as laser candidates a selection of TM complexes that absorb in the green, we have carried out the following program. We have: (1) assembled a doubled Nd-glass laser, (2) conducted an analysis of the thresholds of resonators appropriate to our conditions, (3) assembled resonators optimized from this analysis and designed to enable comparison with the lasing of Rhodamine 6G, and (4) conducted experiments on a selection of TM complex laser candidates. The results of these experiments show that the TM complexes possess either extremely high thresholds as laser materials or that some phenomena such as excited-state absorption (discussed in detail eleswhere in this report) prohibits lasing.

4.2 EXPERIMENTAL SETUP

A block diagram of the experimental setup is shown in Figure 8 along with a photograph in Figure 9. A Korad Q-switched Nd-Glass laser produced 30 ns pulses of greater than 0.5J energy at 1.06μ. A temperature tuned CD*A crystal doubled the frequency of the infrared output to provide 30 ns pulses of up to 0.05J energy for pumping the TM complexes in the resonator. A variable attenuator made up of a selection of neutral density filters provided attenuations to as much as 10^4 of the pump beam.

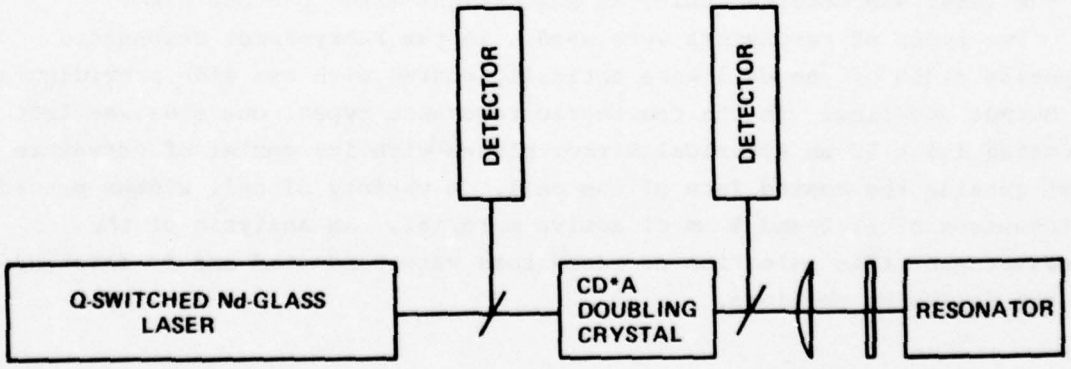

Figure 8. Block Diagram of Experimental Setup

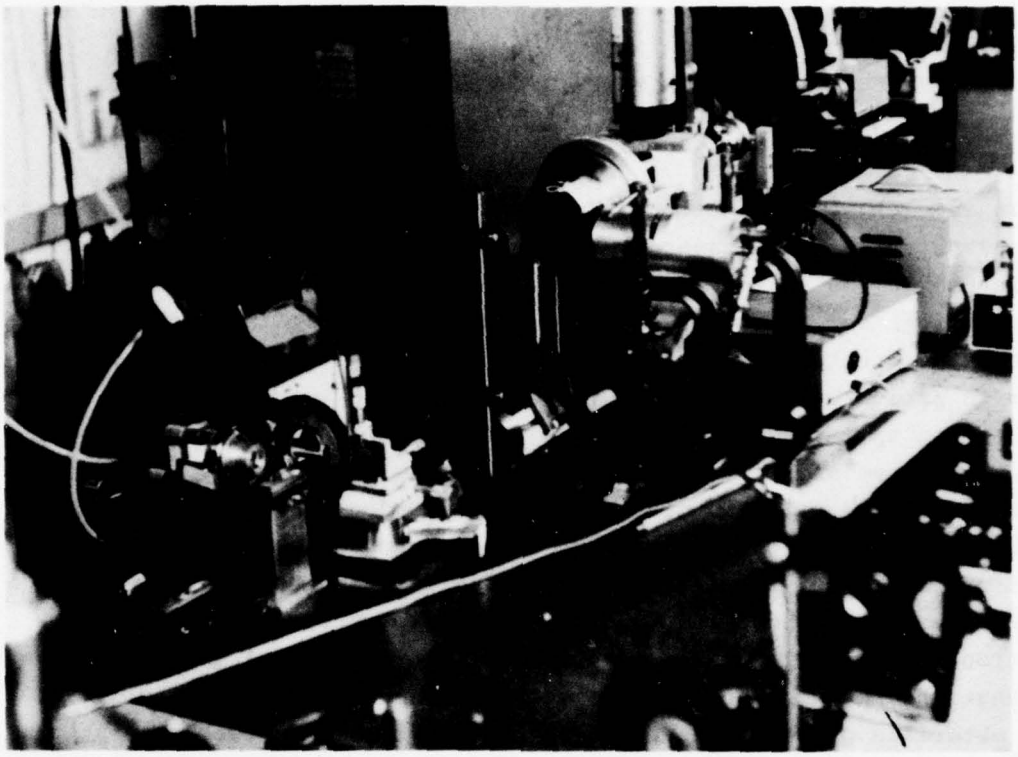

Figure 9. Photograph of Experimental Setup

A photograph of the resonator is shown in Figure 10, and a schematic in Figure 11. The TM complex in solution was contained in cells with plane parallel faces which could be optically coated. The cells were kinematically mounted so that alignment could be made using Rhodamine 6G, the cell removed, and a switch quickly made to a TM complex. Pumping, for the most part, was transverse to avoid pitting of the cell surfaces. For this purpose, two crossed cylindrical lens were adjusted to give a sharply focused line image in the active region of the cell. The output of the laser was observed using an EG&G "Light Mike" photodetector.

Two types of resonators were used. In the Fabry-Perot resonators opposite sides of the cell were optically coated with one side providing a 2% output coupling. In the concentric resonator types, one side was left uncoated and a 50 mm spherical mirror placed with its center of curvature just outside the coated face of the cell. A variety of cell widths provided thicknesses of 1, 2 and 5 mm of active material. An analysis of the thresholds of this selection of resonators were conducted and is described in the following sections.

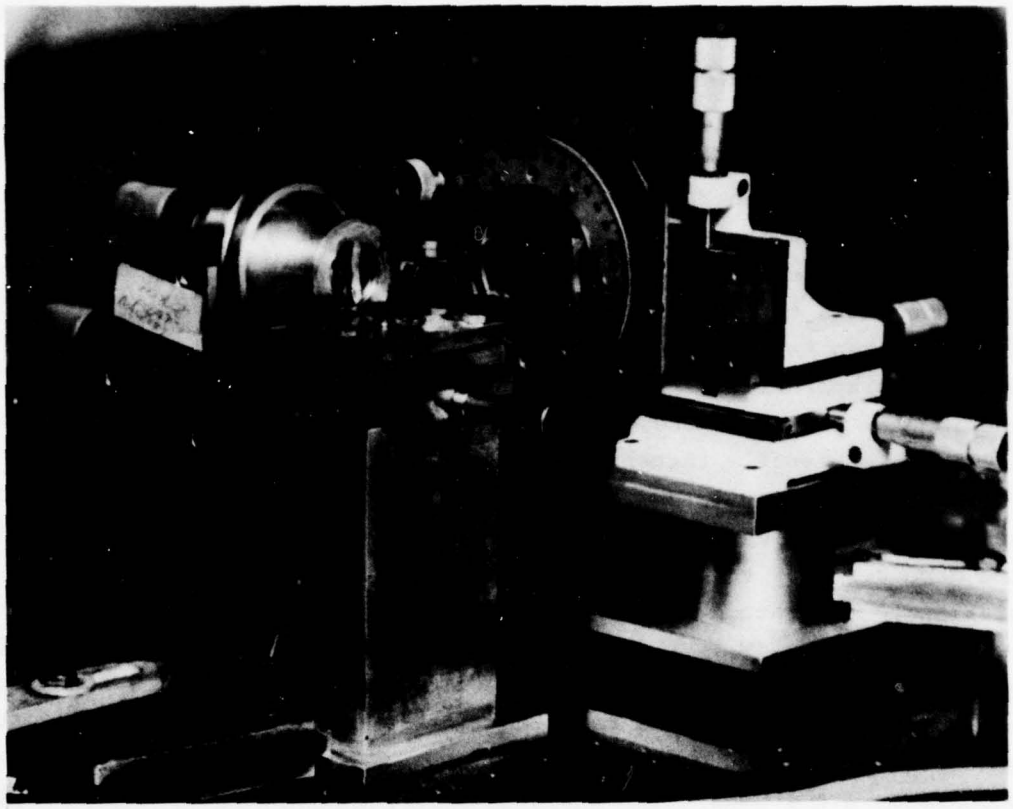

Figure 10. Photograph of Resonator

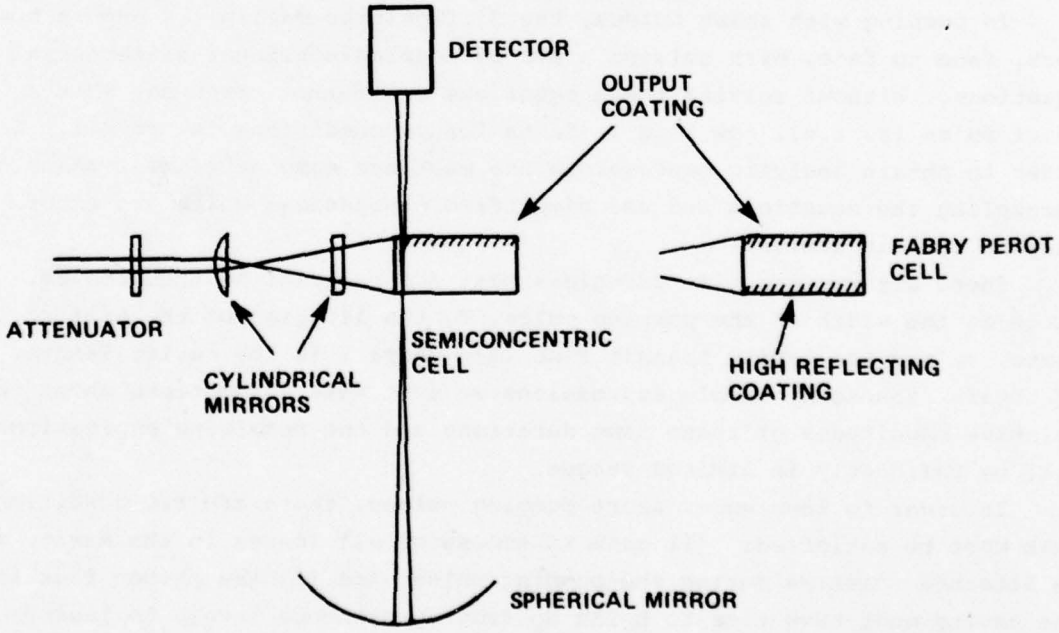

Figure 11. Schematic Diagram of Resonator

4.3 RESONATOR ANALYSIS

It is difficult to predict optical pumping laser thresholds for candidate laser materials with great accuracies. However, it is useful to attempt a calculation taking into account all known factors in order to determine whether the estimated threshold grossly exceeds available pumping energies. On the other hand, if the estimate is not excessive and the candidate fails to lase, one should look for additional factors that have not been taken into account. Further, such an analysis can provide a qualitative appreciation for the significant features of a particular experimental situation and guide the design of resonators consistent with the lowest achievable thresholds.

The analysis of laser thresholds is usually handled using rate equations. These are a coupled set of nonlinear differential equations that relate the time dependence of the electronic excitation and the resulting photon emission to the rate at which pump photons are absorbed, W. Solving those for cw thresholds, $(W_t)_{cw}$ is straightforward since one simply sets all derivatives equal to zero. However, even the cw thresholds can be considered only as estimates since the rate equations are based upon a simplified model and it is hard to anticipate all possible losses. Particularly troublesome are losses which are induced or modified by the electronic population redistribution resulting from optical pumping.

In pumping with short pulses, the difficulties multiply. One is now back, face to face, with solving a set of coupled nonlinear differential equations. Without solving these equations one cannot even say what a short pulse is, i.e., how long it takes for cw conditions to prevail. In order to obtain analytic expressions one must use some artificial means of decoupling the equations and use simplified expressions which are exact only in certain limits.

There are various time durations that are relevant to the problem. There is the width of the pumping pulse, T, the lifetime of the excited state, τ, and the cavity transit time $2\ell/c$ where ℓ is the cavity length. To obtain reasonably simple expressions we must make assumptions about the relative magnitudes of these time durations and the resulting expressions will be valid only in limited ranges.

In order to lase under short pumping pulses, there are two conditions that must be satisfied: (1) gain in excess of all losses in the cavity must be attained sometime during the pumping pulse, and (2) the photon flux in the cavity must have time to build up from spontaneous levels to lasing

levels (i.e., the cw level) before the electronic excitation resulting from the pumping pulse has dissipated too much. Typically the latter represents a change of about 12 orders of magnitude in photon flux. Pumping at a rate corresponding to cw threshold intensity does not assure the attainment of either of these conditions when the pumping pulse is short. We derine the minimum pumping rate $(W_t)_{pulsed}$ required for a pulse width T as the pulsed threshold for the pulse width. Obviously, the pulsed threshold will depend upon the shape of the pumping pulse. To keep the situation reasonably simple, we restrict our calculations to square pumping pulses of amplitude W and width T.

One further restriction limits the validity of the expressions to certain ranges of τ. In our model we make the simplifying assumption that there exists a time duration during which the gain remains essentially constant. From the rate equations we show that such a situation exits for $\tau << T$ and for $\tau >> T$. In the former case, the gain follows the flat pumping pulse. In the latter case, the gain increases monotonically during the pumping pulse and remains flat to within 10% for a time equal to $\tau/10$ afterwards.

Our model then consists simply in a wave originating in the spontaneous emission being amplified the same amount each time it makes a round trip in the cavity. Lasing is said to occur if and when the amplitude of the wave reaches the level it would have attained in cw operation.

This model is shown to follow from the laser rate equations under the assumptions stated. We are able to avoid coupling of the equations in this model since coupling is important only near the end of the photon buildup where we can ignore it.

Consider the microscopic rate equations appropriate for a four-level laser. These equations must be satisfied at each point of the cavity.

$$\frac{dn}{dt} = w - \frac{n}{\tau_r} \frac{c^3}{8\pi\upsilon^2\Delta\upsilon} q - \frac{n}{\tau} \tag{1}$$

$$\frac{dq}{dt} = \frac{n}{\tau_r} \frac{c^3}{8\pi\upsilon^2\Delta\upsilon} (q + \frac{1}{V}) \tag{2}$$

where n and q are, respectively, the inversion density and the photon density, and w is the pump rate density. The quantity V is the volume taken up by the lasing mode, and τ_r is the spontaneous radiative lifetime associated with the lasing transition.

To treat the buildup of running waves in the cavity we transform from the varibles n and q to running wave intensities j and gain coefficients g.

In a typical laser resonator the photon density, q, can be considered as resulting from two traveling waves, one from the left and one from the right. The respective intensities are related to the photon density by:

$$q = \frac{1}{c} (j^+ + j^-) \tag{3}$$

Further we define a quantity, g, which is the gain coefficient:

$$g \equiv \frac{c^2}{8\pi\nu^2\Delta\nu} \frac{n}{\tau_r} \tag{4}$$

In a region where there is no divergence of the beam, Eqs. (1) and (2) become:

$$\frac{dg}{dt} = \frac{c^2}{8\pi\nu^2\Delta\nu} \frac{1}{\tau_r} [w - g (j^+ + j^-)] - \frac{g}{\tau} \tag{5}$$

$$\frac{1}{c} \frac{\partial j^+}{\partial t} + \frac{1}{c} \frac{\partial j^-}{\partial t} + \frac{\partial j^+}{\partial x} - \frac{\partial j^-}{\partial x} = g (j^+ + j^- + \frac{c}{V}) \tag{6}$$

If we neglect spontaneous emission in Eq. (6) we see that:

$$j^+ = j^+(o)e^{gx}; \; j^- = j^-(o)e^{-gx} \tag{7}$$

are solutions as long as g is independent of time. This is consistent with calling g the gain coefficient.

We consider the behavior governed by Eqs. (5) and (6) under a square pumping pulse of amplitude w and width T. Initially, we can neglect the stimulated emission term Eq. (5) and the gain builds up according to:

$$g = \frac{c^2}{8\pi\nu^2\Delta\nu} \frac{\tau}{\tau_r} w \left(1 - e^{\frac{t}{\tau}}\right) \tag{8}$$

If the pulse is long enough, the stimulated emission contribution results in the steady-state gain

$$g_\infty = \frac{c^2}{8\pi\nu^2\Delta\nu} \frac{\tau}{\tau_r} w \frac{1}{1 + \frac{c^2}{8\pi\nu^2\Delta\nu} \frac{\tau}{\tau_r} (j^+ + j^-)} \tag{9}$$

To analyze the buildup of the photon flux we must consider details of the laser resonator. Consider a resonator shown schematically in Figure 12. The active region is restricted to a thin film of thickness $\Delta\ell$ at the plane output mirror of reflectivity R. We consider a volume of area ΔA and $\Delta\ell$ uniformly illuminated and for simplicity we assume j is constant over the area ΔA.

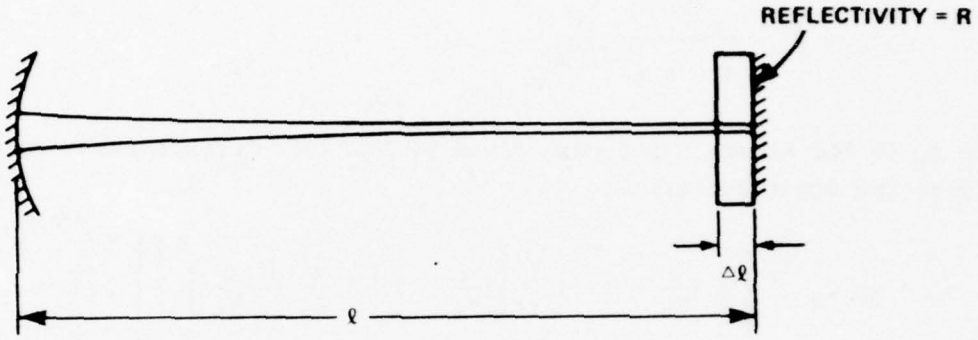

Figure 12. Resonator Model for Calculations

If the spontaneous emission contributes equally to j^+ and j^- we can separate Eq. (6) into individual equations for j^+ and j^- giving:

$$\frac{1}{c}\frac{\partial j^{\pm}}{\partial t} \pm \frac{\partial j^{\pm}}{\partial x} = g\left(j^{\pm} + \frac{1}{2}\frac{c}{V}\right) \tag{10}$$

Consider the leading edge of a wave traveling to the right that builds up from the spontaneous emission starting from zero at the left side of the active region. For time durations over which g doesn't change much, this is given in the active region by Eq. (10).

$$j \approx \frac{c}{2V}\left(e^{gx} - 1\right) \tag{11}$$

After one complete pass through the resonator this becomes:

$$j_1 = \frac{cR}{2V}\left(e^{2g_1\Delta\ell} - 1\right) \tag{12}$$

For subsequent passes:

$$j_n = \frac{c}{2V} R \left(e^{2g_n \Delta \ell} - 1 \right) + j_{n-1} R e^{2g_n \Delta \ell} \tag{13}$$

By setting $j_n = j_{n-1}$ we obtain the steady state corresponding to cw operation:

$$j_\infty = \frac{c}{2V} R \frac{e^{2g_\infty \Delta \ell} - 1}{1 - R e^{2g_\infty \Delta \ell}} \tag{14}$$

where g_∞ is the steady state gain given by Eq. (9). Simultaneous solutions of these two equations gives:

$$j_\infty = \frac{c}{2V} Q_o \frac{\tau_r}{\tau} \left\{ \frac{1}{2} \left(\frac{w}{w_t} - 1 \right) + \frac{1}{2} \left[\left(\frac{w}{w_t} - 1 \right)^2 + \frac{4}{Q_o} \frac{\tau}{\tau_r} \frac{w}{w_t} \right]^{\frac{1}{2}} \right\} \tag{15}$$

where Q_o is the number of modes in the gain bandwidth given by:

$$Q_o = \frac{8\pi\nu^2 \Delta\nu}{c^3} \tag{16}$$

and w_t is the cw threshold pumping rate given by:

$$w_t = \frac{8\pi\nu^2 \Delta\nu}{c^2} \frac{\tau_r}{\tau} \frac{1}{2\Delta\ell} \ln\left(\frac{1}{R}\right) \tag{17}$$

Above this threshold:

$$j_\infty = \frac{c}{2V} Q_o \frac{\tau_r}{\tau} \left(\frac{w}{w_t} - 1 \right) \tag{18}$$

(where Q_o may be on the order of 10^{12}) and below threshold:

$$j_\infty \approx \frac{c}{2V} \frac{\frac{w}{w_t}}{1 - \frac{w}{w_t}} \tag{19}$$

It follows from Eq. (18) that the threshold gain is given by:

$$g_t = \frac{1}{2\Delta\ell} \ln\left(\frac{1}{R}\right) \tag{20}$$

Related to the threshold pumping rates is the threshold inversion concentration, n_t, given by:

$$n_t = \frac{8\pi\nu^2\Delta\nu}{c^2} \frac{\tau_r}{2\Delta\ell} \ln\left(\frac{1}{R}\right) = w_t \tau \tag{21}$$

The calculated threshold inversion should be comfortably below the concentration of active centers if lasing is to be expected.

If we assume uniform pumping of the volume, $\Delta v = \Delta\ell\Delta A$, the total cw threshold pumping rate, w_t, because;

$$W_t = \frac{4\pi\nu^2\Delta\nu}{c^2} \frac{\tau_r}{\tau} \ln\left(\frac{1}{R}\right) \Delta A \tag{22}$$

Constraints on the area ΔA are imposed by details of the resonator. The pumped region must be contained within the mode volume. For a Faby-Perot cavity (plane mirrors), the area must be large enough to limit the diffraction losses. These should be no greater than the losses due to output coupling. If the diffraction losses are to be on the order of 2%, the results of Fox and Li[23] give:

$$\Delta A \approx 6 \lambda\ell \tag{23}$$

For the lowest order mode of two semiconcentric cavities with spherical mirror of radius, $\mathcal{R}$:

$$\Delta A = 2\ell \left(\frac{\mathcal{R}}{\ell} - 1\right)^{\frac{1}{2}} \tag{24}$$

In order to lase under short pumping pulses there are two conditions that must be satisfied: (1) threshold gain [Eq. (20)] must be attained sometime during the pumping pulse, and (2) the photon flux in the cavity

must have time to build up from spontaneous levels [Eq. (19)] to lasing levels [Eq. (18)] before the effect of the pumping pulse (electronic excitation) has dissipated too much.

Consider the first condition. The gain builds up according to Eq. (8), giving at the end of a pump pulse of width, T:

$$g = g_t \frac{w}{w_t} \left(1 - e^{-\frac{T}{\tau}}\right) \tag{25}$$

Therefore, to attain threshold gain:

$$W \geq \frac{W_t}{1 - e^{-T/\tau}} \tag{26}$$

If $T >> \tau$ we have essentially the cw situation:

$$W \geq W_t = \frac{4\pi\nu^2\Delta\nu}{c^2} \ln\left(\frac{1}{R}\right) \frac{\tau_r}{\tau} \Delta A \tag{27}$$

and for $T << \tau$:

$$W \geq \frac{\tau}{T} W_t = \frac{4\pi\nu^2\Delta\nu}{c^2} \ln\left(\frac{1}{R}\right) \frac{\tau_r}{\tau} \Delta A \tag{28}$$

The second condition imposes more stringent constraints. This situation is most easily analyzed in the limit where $\tau << 2\ell/c$. In this limit the gain can be considered constant during almost the entire buildup of the photon flux and the difference equation, Eq. (13), can be solved easily giving:

$$j_n = \frac{c}{2V} \left(R\, e^{2g\Delta\ell} - R\right) \frac{1 - R^n\, e^{2gn\Delta\ell}}{1 - R^{2g\Delta\ell}} \tag{29}$$

with the substitution

$$R\, e^{2g\Delta\ell} = \left(\frac{1}{R}\right)^{\left(1 - \frac{1}{w_t}\right)} = R^{\left(1 - \frac{w}{w_t}\right)}$$

obtained from Eqs. (20) and (25) this becomes:

$$j_n = \frac{c}{2V}\left[R^{\left(1-\frac{w}{w_t}\right)} - R\right]\frac{R^{n\left(1-\frac{w}{w_t}\right)} - 1}{R^{\left(1-\frac{w}{w_t}\right)} - 1} \tag{30}$$

if

$\frac{w}{w_t} > 1$ and $n >> 1$:

$$j_n \approx \frac{c}{2V}\frac{R^{\left(1-\frac{w}{w_t}\right)} - R}{R^{\left(1-\frac{w}{w_t}\right)} - 1} R^{n\left(1-\frac{w}{w_t}\right)} \tag{31}$$

If lasing is to occur, the number of passes must be large enough for j_n to approach the steady state level, j_∞. This requires a number of passes given by:

$$n = \frac{1}{\frac{w}{w_t} - 1}\frac{\ln\left[\frac{R^{\left(1-\frac{w}{w_t}\right)} - 1}{R^{\left(1-\frac{w}{w_t}\right)} - R} Q_o \frac{\tau_r}{\tau}\left(\frac{w}{w_t} - 1\right)\right]}{\ln\left(\frac{1}{R}\right)} \tag{32}$$

Equation (32) can be looked at from two different viewpoints. If a step function pump pulse of unlimited duration is applied, then a delay, δt, occurs before the onset of lasing given by:

$$\delta t = n\frac{2\ell}{c} \tag{33}$$

This delay for several values of R is given in Figure 13.

On the other hand, if a square pulse of duration T is applied, then lasing will occur only if $T \geq \delta t$. For the shortest pulses this would require $w/w_t >> 1$. The lowest pumping rate required to obtain lasing under these conditions is then the threshold for a pulse of duration T, whereas W_t is the cw threshold. Equation (32) can then be used to calculate the pulsed threshold and this data is given in Figure 14 for several values of R.

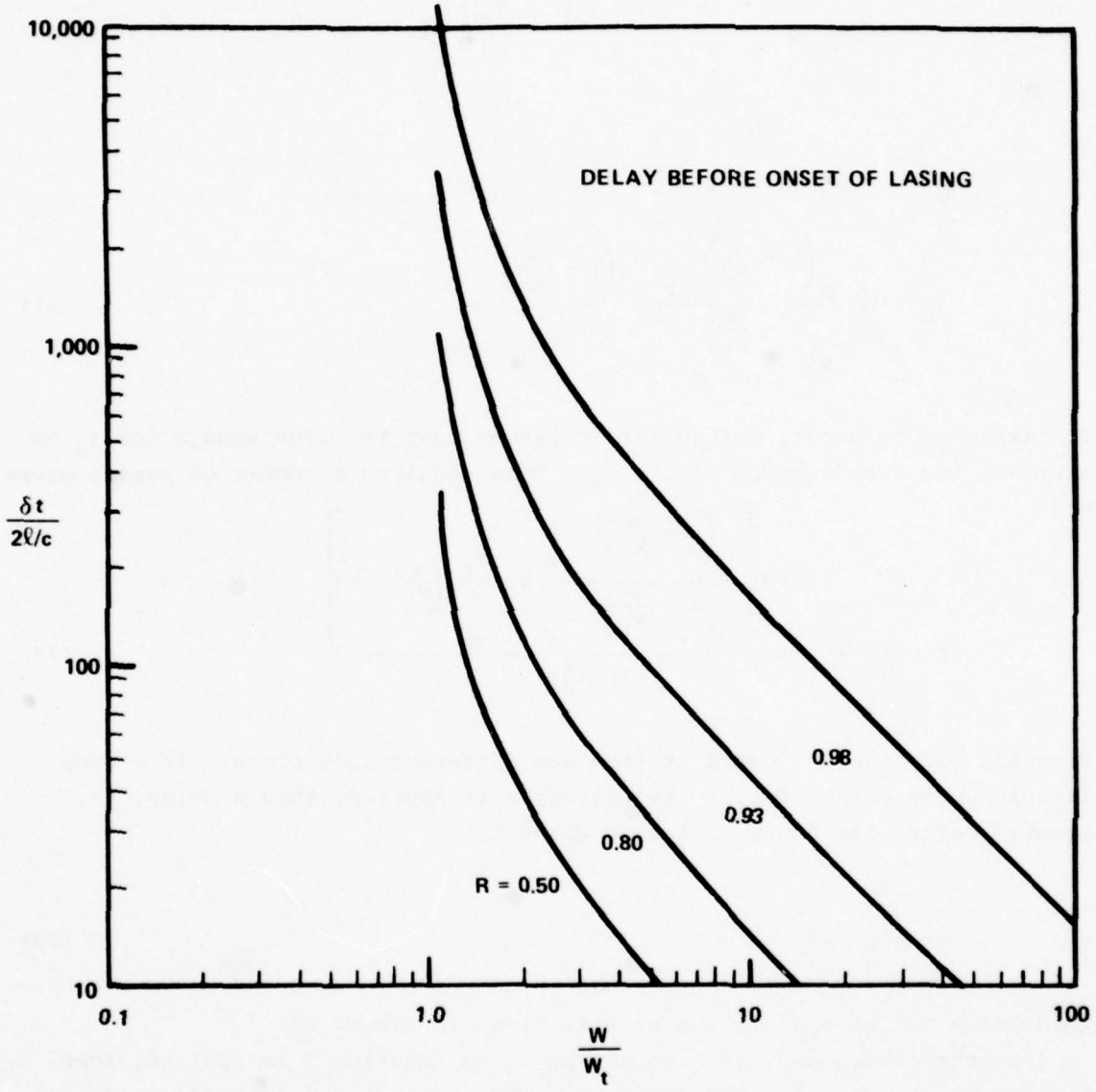

Figure 13. Delay Before Onset of Lasing

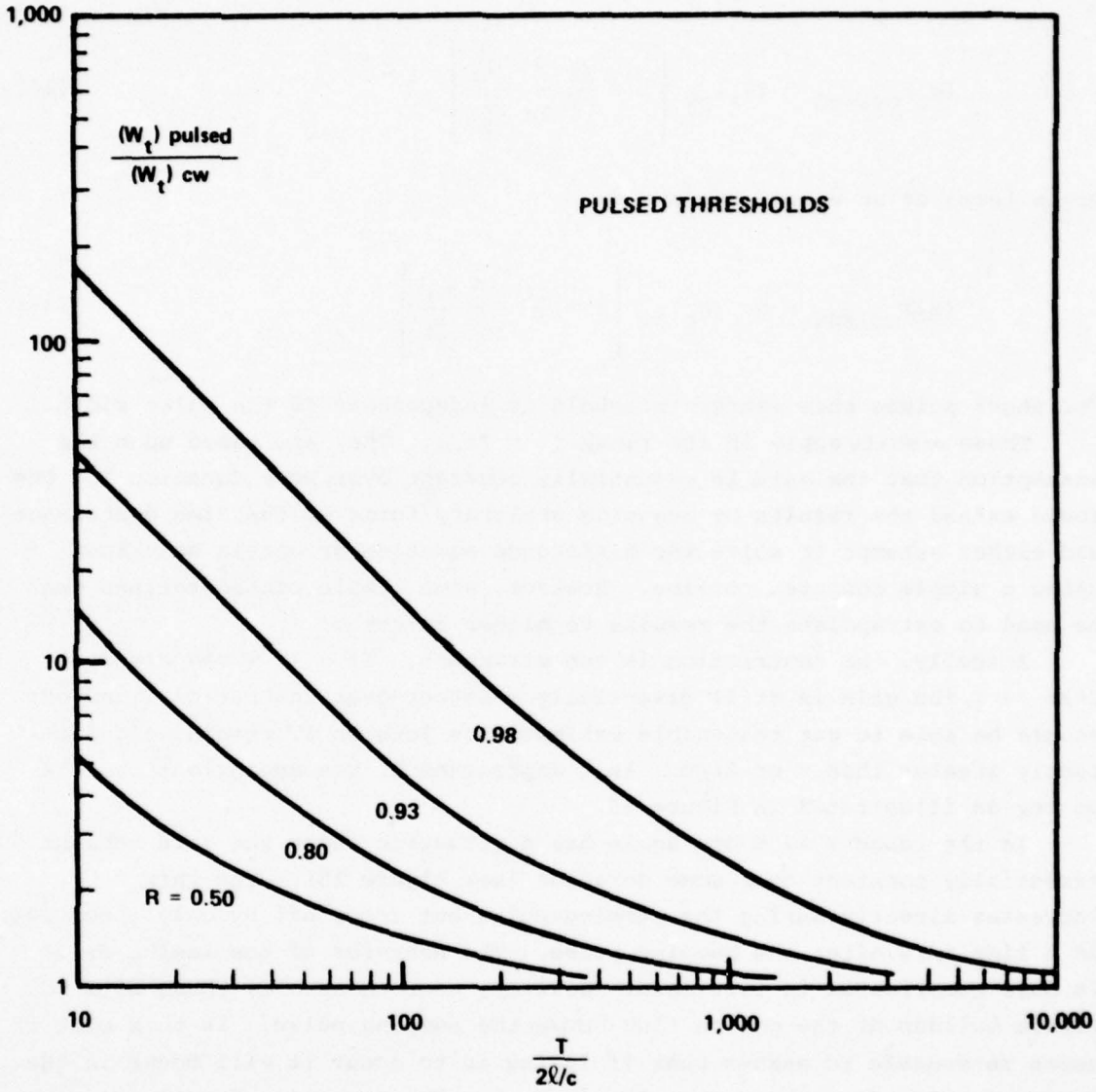

Figure 14. Pulsed Thresholds

Since Q_o is typically on the order of 10^{12}, we can obtain a simplified version of Eq. (32) by neglecting the other factors in the argument of the ln function giving:

$$(W_t)_{pulsed} \approx (W_t)_{cw} \left[1 + \frac{2\ell}{cT} \frac{\ln Q_o}{\ln (\frac{1}{R})} \right] \tag{34}$$

Or in terms of an energy threshold:

$$(E_t)_{pulsed} = h\nu (W_t)_{cw} \left[T + \frac{2\ell}{c} \frac{\ln Q_o}{\ln (\frac{1}{R})} \right] \tag{35}$$

For short pulses this energy threshold is independent of the pulse width.

These results apply in the range $\tau << 2\ell/c$. They are based upon the assumption that the gain is essentially constant over some duration T. One could extend the results by assuming arbitrary forms of the time dependence and either attempt to solve the difference equation or obtain solutions using a simple computer routine. However, some simple considerations can be used to extrapolate the results to higher values of τ.

Actually, the restriction is too stringent. If $\tau << T$ and also $2\ell/c << T$, the gain is still essentially constant over the period T and one should be able to get reasonable estimates as long as δT remains significantly greater than τ or $2\ell/c$. As τ approaches T, the approximation gets poorer as illustrated in Figure 15.

In the range $\tau >> T$ one again has a situation where the gain remains essentially constant over some duration (see Figure 15). The gain increases linearly during the pumping pulse but drops off by only about 10% in a time $\tau/10$ after the pumping pulse. The behavior of the lasing delay is more complicated in this case. However, near threshold, there will be little buildup of the photon flux during the pumping pulse. In this case it seems reasonable to assume that if lasing is to occur it will occur in the interval $\tau/10$ after the pump pulse is over. For purposes of estimating thresholds, then, we adopt the somewhat arbitrary square pulse approximation that a gain given by Eq. (25) exists for a time $\tau/10$. We accordingly modify the relations already obtained for shorter pulses.

From Eq. (25) the appropriate substitution to be made in Eq. (29) is given by:

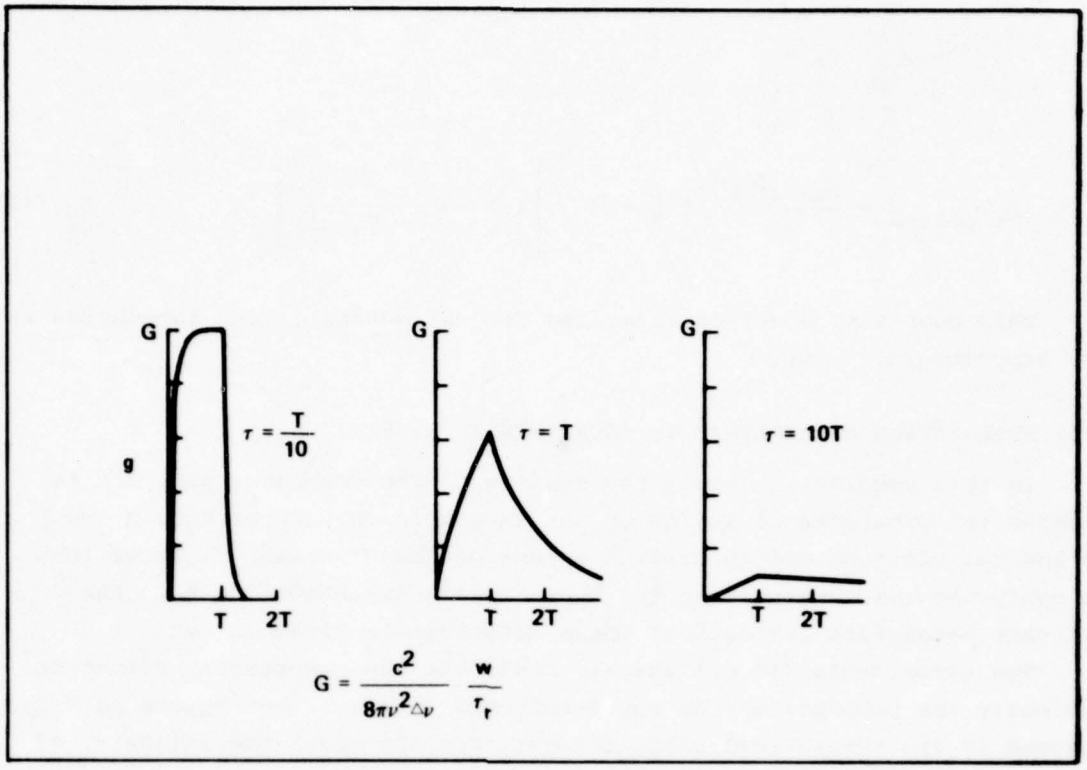

Figure 15. Time Dependence of Gain for Various Ranges of Excited State Lifetime

$$R\, e^{2g\Delta\ell} = \left(\frac{1}{R}\right)^{\left(\frac{w}{w_t}\frac{T}{\tau} - 1\right)} \tag{36}$$

The number of passes, n, becomes:

$$n = \frac{1}{10}\,\frac{\tau}{2\ell/c} \tag{37}$$

The threshold for pulsed operation then becomes:

$$(W_t)_{pulsed} = (W_t)_{cw}\,\frac{\tau}{T}\left[1 + 10\,\frac{2\ell}{c\tau}\,\frac{\ln Q_o}{\ln\left(\frac{1}{R}\right)}\right] \tag{38}$$

giving an energy threshold:

$$(E_t)_{pulsed} = \frac{4\pi h\ \nu^3 \Delta\nu}{c^2} \ln \frac{1}{R}\ \Delta A\ \tau_r \left[1 + 10\ \frac{2\ell}{c\tau}\ \frac{\ln Q_o}{\ln (\frac{1}{R})}\right] \tag{39}$$

This completes a set of relations for estimating lasing thresholds in our experimental setup.

4.4 APPLICATION OF ANALYSIS TO EXPERIMENTAL SITUATION

In this section, we apply the results of the resonator analysis to examine the prospects of lasing by the TM complexes. To provide a check on the calculations and to provide a test of the experimental situation, we apply the same analysis to the known lasing dye Rhodamine 6G. The relevant parameters for each of these materials is given in Table 1.

The experiments did not exactly duplicate the theoretical situation. Obviously the pump pulse from the Q-switched laser was not square as assumed in the theoretical calculations. For the width and intensity of the equivalent square wave we take the half width and peak intensity of the experimental pulse. Further it is not clear how well the pumped region was superimposed upon the lasing mode volume. We simply aligned the resonators to give the lowest achievable thresholds for Rhodamine 6G. The lack of ideal conditions in both of these situations would increase the experimentally observed thresholds, but probably less than an order of magnitude.

TABLE 1

LASER MATERIAL PROPERTIES AT ROOM TEMPERATURE

	λ	$\Delta\lambda$	τ_r	τ
Rhodamine 6G	0.57 μm	0.05 μm	10^{-9}s	10^{-9}s
Typical TM Complex	0.65 μm	0.08 μm	10^{-5}s	(1-5) x 10^{-7}s

The parameters for the various resonators are given in Table 2, and the calculated energy thresholds for lasing are given in Table 3. In general, the calculated thresholds are much lower than the experimentally available pump energies. The thresholds for the TM complexes are approximately 100X those for Rhodamine 6G. The threshold inversion concentrations

for each of the lasing materials depend upon the interior thickness of the cell and are given in Table 4.

TABLE 2

RESONATOR PARAMETERS

$R \approx 0.98$

$Q_o \approx 10^{12}$

$T \approx 30 \times 10^{-9}$s

FABRY-PEROT			
	$\Delta\ell$	ℓ	
Cell 1	1 mm	3 mm	
Cell 2	2 mm	4 mm	
Cell 3	3 mm	9 mm	
SEMICONCENTRIC			
	$\Delta\ell$	ℓ	$\mathscr{R}$
Cell 1	1 mm	45 mm	50 mm
Cell 2	2 mm	45 mm	50 mm
Cell 3	3 mm	45 mm	50 mm

TABLE 3

LASER THRESHOLDS (μJ)

	FABRY PEROT			SEMICONCENTRIC
	1 mm	2 mm	5 mm	
Rhodamine 6G	0.006	0.016	0.08	0.07
TM Complex	1.0	3.0	7.5	10.5
Ratio	167	187	93	160

TABLE 4

LASER CANDIDATES INVESTIGATED

TM COMPLEX	MOLARITY	α	CONCENTRATION	APPROXIMATE THRESHOLD INVERSION		
				1	2	5 mm CELL
1. Rhodamine 6G	4.0×10^{-3}M	10 cm^{-1}	2.4×10^{18} cm^{-3}	3.6×10^{13}	1.8×10^{13}	7.2×10^{12} cm^{-3}
2. $Ru(bipy)_3Cl_2$	5.7×10^{-3}M	10 cm^{-1}	3.4×10^{18}	3.6×10^{17}	1.8×10^{17}	7.2×10^{16}
3. $Ru(phen)_3Cl_2$	7.4×10^{-3}M	10 cm^{-1}	4.5×10^{18}			
4. $Ru(5,6\text{-}Me_2phen)$		10 cm^{-1}				
5. $Ru(\ell_2phen)_3Cl_2$	1.87×10^{-2}M	100 cm^{-1}	1.1×10^{19}			
	1.87×10^{-3}M	10 cm^{-1}	1.1×10^{18}			
6. $Ru(\ell_2bipy)_3Cl_2$	0.92×10^{-2}M	100 cm^{-1}	5.1×10^{18}			
	0.92×10^{-3}M	10 cm^{-1}	5.1×10^{17}			
7. $Ru(Me_4\text{-phen})$		10 cm^{-1}				

4.5 EXPERIMENTAL RESULTS

The various resonators were initially aligned and lasing was obtained using Rhodamine 6G. The pumping beam was then attenuated in steps and the alignment touched up to optimize lasing at each step. Commonly, attenuations of 10^3 were possible before lasing was no longer possible and with the semiconcentric resonator, attenuations of 10^4 were attained. This indicates that we were able to pump Rhodamine 6G as much as 10^4 × threshold. A threshold at 1 μJ for Rhodamine 6G in the concentric resonator was observed which is in reasonable order of magnitude agreement with the calculated value of 0.07 μJ.

After establishing the alignment using Rhodamine 6G, the kinematically mounted cells were removed and the Rhodamine 6G replaced by a solution of a TM complex from Table 4; no lasing was observed from any of these.

4.6 DISCUSSION

In the lasing experiments we have pumped selections of TM complexes at 10^4 times the threshold of Rhodamine 6G. At these pumping levels, calculations indicate that we should have saturated the inversion and exceeded estimated thresholds by as much as two orders of magnitude. This would indicate that unknown factors either result in excessively large thresholds or prohibit lasing altogether. A candidate, as discussed elsewhere in this report, is excited state absorption.

If the problem with lasing of the TM complex is excited state absorption, experiments can establish this and a detailed study may reveal special cases where lasing is possible. The difficulty may be due to some unknown intrinsic loss that simply raises the thresholds a couple orders of magnitude. If this is the case, there are several things that might be done to improve matters.

The required threshold inversion densities could be reduced by using thicker cells. This would permit exploiting more of the available pump energy before saturation effects occur. In order to use this approach successfully, one may have to employ special techniques for stretching the pump-laser beam into a long line.

The other approach would be to attempt to increase the cw threshold in some way. Cooling the TM complex is capable of reducing the excited-state lifetime by a factor of 10X to 20X and should decrease the pulsed thresholds accordingly.

5. CONCLUSION AND RECOMMENDATION

As discussed in the Introduction, the distinguishing characteristic of the luminescence of TM complexes is their relatively long radiative lifetime. It is this feature which clearly separates these materials from purely organic laser dyes and which make them attractive laser candidates. Paradoxically, we now think it is the forbidden nature of the radiative transition which makes laser action difficult or perhaps impossible to achieve in TM complexes. This is because the partially forbidden emission must compete with allowed excited-state absorption in order to achieve gain.

To see this more clearly, consider the general molecular energy level scheme shown in Figure 16. The states labeled S are spin paired singlets and those labeled T are spin triplets. We assume the ground state is S_o. Strictly speaking, this scheme is appropriate for molecules containing light atoms in which spin-orbit coupling is small and spin is a good quantum number, but it does provide a convenient point of departure for understanding the behavior of TM complexes. Organic dyes, comprised of light atoms, can be effectively pumped via the $S_n \leftarrow S_o$ transitions, and in some of these, particularly those containing carbonyl functions, T_1 can be readily populated by rapid intersystem crossing. It is the $T_1 \rightarrow S_o$ phosphorescent transition which is analogous to the partially forbidden emission of TM complexes, and, as with TM complexes, there is no kinetic difficulty with producing a population inversion in a four-level phosphorescent material. One reason, among others, why phosphorescent lasers are unknown lies in the following term in the gain equation.

$$\exp\left[N_{T_1}\left(\sigma_{T_1 \rightarrow S_o} - \sigma_{T_n \leftarrow T_1}\right)\right]$$

The cross section for $T_n \leftarrow T_1$ absorption, a spin-allowed process, will always overwhelm the cross section for stimulated $T_1 \rightarrow S_o$ emission, a spin-forbidden process, so that gain will be negative for phosphorescent molecules. The bandwidth of molecular transitions in condensed media and density of excited states in complex molecules insures that a "window" will not fortuitously exist in the T_1 absorption spectrum at the frequencies of phosphorescence. Molecules for which extensive $T_n \leftarrow T_1$ absorption spectra have been measured confirm this.

The situation in TM complexes is similar but not identical. Extensive spin-orbit coupling which is encountered in the second and third row

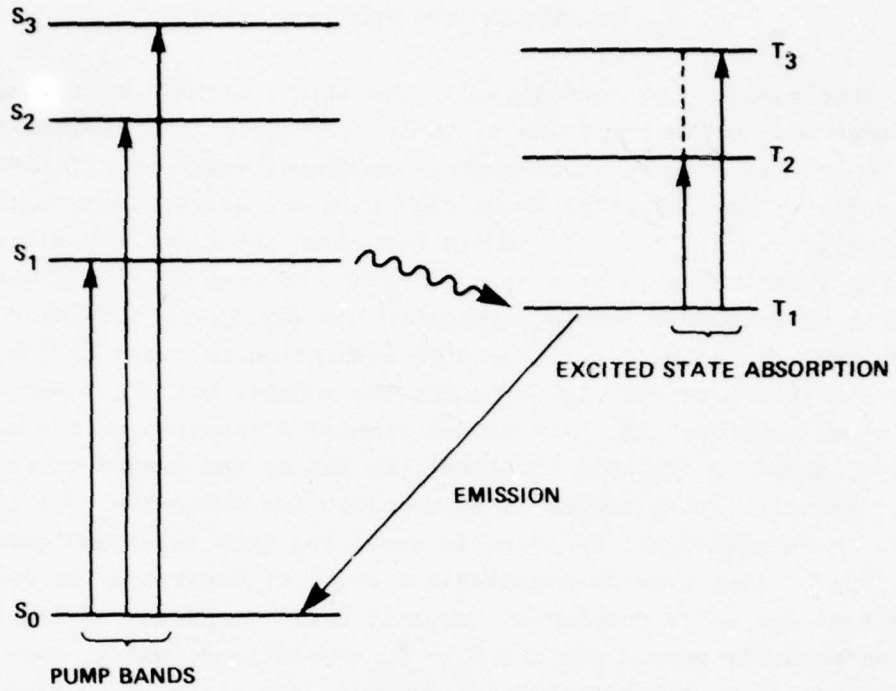

Figure 16. Simplified Energy Level Diagram Appropriate for Modules Containing First Row Atoms

transition metals, to a large extent blurs state spin labels through extensive mixing. It has been argued that spin labels are entirely inappropriate for d-π^* excited states of Ru(II) complexes.[10] Nevertheless, the evidence is abundant that a vestige of the spin-selection rule remains. The radiative lifetime of Ru(II) complexes is approximately 10^{-5}s, a factor of 10^3 less than that expected for a fully allowed transition. Conversely, in favorable cases, the d-π^* states responsible for emission can be seen in absorption as a very weak feature on the red edge of a much more intense band. Symmetry arguments do not explain the partially forbidden nature of these transitions Similarly, the first absorption of $Rh(P{=}P)_2Cl$ is quite weak ($\varepsilon \sim 200$ $cm^{-1}\ell^{-1}$ mole) which is consistent with its long lifetime (28.5 μs). In this case the emitting level is clearly associated with a component of a $^3A_{2u}$ state which is split by spin-orbit coupling. The analogous transition in $Ir(P{=}P)_2Cl$ is about a factor of 10 more intense, and, because of the relatively narrow emission bandwidth of the Ir(I) complex., we considered this material to have the best chance of piercing the ubiquitous excited-state absorption (that is, $\sigma_{T_1 \leftarrow S_o} > \sigma_{T_n \leftarrow T_1}$). However, the small Stokes

shift in $Ir(P{=}P)_2Cl$ leads to extensive ground state absorption losses which may prevent lasing. In the metalloporphyrins, which have an enormous Stokes shift and an even more narrow emission bandwidth, lasing is probably prevented by the highly forbidden nature of the transition ($\tau = 10^{-4}$s).

The common theme encountered among TM complexes is that weak emission must compete against strong absorption from the emitting level. The density of states and strong mixing of states which lie close in energy make it nearly certain that transitions analogous to $T_n \leftarrow T_1$ will be as prevalent in TM complexes as in organic dyes. It can reasonably be asked whether such losses are present in fluorescent laser dyes. In these cases the radiative transition is fully allowed ($S_1 \rightarrow S_o$) and has a much higher probability of showing gain ($^{\sigma}S_1 \rightarrow S_o > {}^{\sigma}S_n \leftarrow S_1$) than in TM complexes. Nevertheless, losses due to $S_n \leftarrow S_1$ absorption have been shown to prevent lasing in pyrene excimers[6] and to diminish gain in crysylviolet.[7] It is quite likely that this loss plays an important but almost neglected role in the spectroscopy of laser dyes.

While it seems reasonable to attribute the lack of laser action to excited state absorption, the point can only be established experimentally. Thus, we strongly recommend that appropriate excited-state absorption measurements be carried out so as to either definitively rule out laser action in TM complexes or to reestablish this possiblility in what appeared to be a promising new class of laser materials.

6. REFERENCES

1. L. Pekkarinen and H. Linschitz, J. Am. Chem. Soc. 82, 2407 (1960).
2. B.M. Dzhagarov, Y.I. Kozlov, A.P. Simonov, and G.P. Gurinovich, Opt. Spectr. 32, 444 (1972).
3. M.P. Tsvirko, V.V. Sapunov and K.N. Soloveo, Opt. Spectr. 34, 635 (1973).
4. A.D. Kirk, P.E. Hoggard, G.B. Porter, M.G. Rockley and M.W. Windsor, Chem. Phys. Let. 37, 199 (1976).
5. B. Bensasson, C. Salet and V. Balzani, J. Am. Chem. Soc. 98, 3722 (1976).
6. J. Langelaar, Appl. Phys. 6, 61 (1975).
7. E. Sahar and I. Wieder, Chem. Phys. Let. 23, 518 (1973).
8. J. Shah and R.F. Leheny, Appl. Phys. Let. 24, 562 (1974); IEEE Quan. Elec. 11, 70 (1975).
9. G.A. Crosby, Accounts Chem. Res. 8, 231 (1975).
10. G.A. Crosby, K.W. Hipps and W.Hu Elfring, Jr., J. Am. Chem. Soc. 96, 629 (1974).
11. H. Samelson, A. Lempicki and C. Brecher, J. Chem. Phys. 40, 2553 (1964).
12. R.E. DeSimone and R.S. Drago, Inorg. Chem. 8, 2517 (1969).
13. R.J. Watts, G.A. Crosby and J.L. Sansregret, Inorg. Chem. 11, 1474 (1972).
14. R. Ballardini, G. Varani, L. Moggi, V. Balzani, K.R. Olson, F. Scandola and M.Z. Hoffman, J. Am. Chem. Soc. 97, 728 (1975).
15. J.N. Demas, E.W. Harris, C.M. Flynn, Jr. and D. Diemente, J. Am. Chem. Soc. 97, 3838 (1975).
16. G.L. Geoffroy, M.S. Wrighton, G.S. Hammond and H.B. Gray, J. Am. Chem. Soc. 96, 3105 (1974).
17. M. Wrighton and D.L. Morse, J. Am. Chem. Soc. 96, 998 (1974).
18. D. Eastwood and M. Gouterman, J. Mol. Spec. 30, 437 (1969).
19. Ibid. 35, 359 (1970).
20. D. Magde, M.W. Windsor, D. Holten and M. Gouterman, Chem. Phys. Let. 29, 183 (1974).
21. W.G. Herkstroeter in "Creation and Detection of the Excited State," Marcel Dekker, Inc., New York (1971).
22. A. Lempicki, H. Samelson and C. Brecher, J. Chem. Phys. 41, 1214 (1964).
23. A.G. Fox and Tingye Li, Bell System Tech. J. 40, 453 (1961).

APPENDIX A

EXCITATION POLARIZATION OF LUMINESCENT IRIDIUM(I) AND RHODIUM(I) PHOSPHINE COMPLEXES

[Reprinted from Inorganic Chemistry 17, 3180 (1978).]

Contribution from GTE Laboratories Inc.,
Waltham, Massachusetts 02154

Excitation Polarization of Luminescent Iridium(I) and Rhodium(I) Phosphine Complexes

LEONARD J. ANDREWS

Received April 17, 1978

Excitation polarization of the luminescent complexes $[M(P{=}P)_2]Cl$ and $[M(P{-}P)_2]Cl$ [M = Ir(I), Rh(I); P=P = *cis*-1,2-bis(diphenylphosphino)ethylene; P—P = 1,2-bis(diphenylphosphino)ethane] have been measured in 1-propanol at −165 °C. Detailed spectral assignments are made in terms of the spin–orbit coupling model which has evolved to describe the absorption of d^8 metal ions complexed with π-acceptor ligands. Comparisons are made with an earlier magnetic circular dichroism study of these complexes.

Introduction

There has been considerable effort over the years devoted to understanding the electronic absorption spectra of d^8 transition-metal ions complexed with π-acceptor ligands.[1-10] By far most attention has focused on the $Ni(CN)_4^{2-}$ and $Pt(CN)_4^{2-}$ anions. The intense lowest energy absorption bands in square-planar tetracyano complexes were originally interpreted by Gray and Ballhausen[1] as metal to ligand charge-transfer (MLCT) transitions from the highest occupied metal d orbitals to the lowest unoccupied ligand π orbital ($a_{2u} \leftarrow d$). Piepho et al.[3] refined this model on the basis of magnetic circular dichroism (MCD) studies to include the effects of spin–orbit coupling. Further MCD studies on a variety of Pt(II) complexes by Ici and Mason[5] and single-crystal polarized absorption measurements on $Ni(CN)_4^{2-}$ by Cowman, Ballhausen, and Gray[4] and on $Pt(CN)_4^{2-}$ by Cowman and Gray[9] were interpreted using the spin–orbit coupling model of Piepho et al.[3] On the other hand, Xα scattered-wave calculations on $Pt(CN)_4^{2-}$ have led Interrante and Messmer[6] to question several assignments principally due to their calculated reordering of metal d-orbital energies.

Recently, this work on tetracyano complexes has been used as a basis for interpreting the absorption of square-planar Rh(I) and Ir(I) complexes.[8,10,11] In particular, MCD spectra of $[M(P{=}P)_2]Cl$ and $[M(P{-}P)_2]Cl$ [M = Rh(I), Ir(I); P=P = *cis*-1,2-bis(diphenylphosphino)ethylene; P—P = 1,2-bis(diphenylphosphino)ethane] have been used by Geoffroy et al.[10] to make detailed spectral assignments. As pointed out by Gray,[4,9] it is desirable to complement MCD data with absorption polarization to provide a firm basis for assignments. We have done this for the above complexes by taking advantage of their photoluminescence at low temperatures in rigid organic glasses.

By use of the method of photoselection,[12] polarized excitation spectra were recorded of dilute solid solutions in 1-propanol. For luminescent molecules, photoselection is a convenient and powerful method for obtaining polarizations which does not require single crystals. The disadvantage of the technique is that excitation polarizations are measured relative to the orientation of the emission oscillator and are not directly related to the molecular framework. We will show, however, for the particular cases studied here, that transition moment orientations relative to molecular coordinates (in-plane or out-of-plane) can be inferred from the sign and magnitude of the excitation polarizations.

Experimental Section

Polarization Measurements. A 150-W xenon arc dispersed with a 0.25-m Jarrel Ash monochromator (82-410) was used for excitation and a 0.5-m Perkin-Elmer monochromator (E-1), equipped with an RCA C3103A photomultiplier, was used for detection. The slits of the excitation monochromator were set at 0.5 mm which corresponds to ~1.5 nm spectral resolution. The excitation beam was passed through a Glan Thompson polarizer and emission was detected through a Polaroid polarizer. Excitation and emission beams were at right angles. Samples were contained in a 0.5-cm quartz tube held in a quartz Dewar and cooled with N_2 gas. A thermocouple was immersed directly in the sample. Sample concentration was $\sim 1 \times 10^{-4}$ M.

Polarization (P) is defined

$$P \equiv (I_{\parallel} - I_{\perp})/(I_{\parallel} + I_{\perp})$$

where $I_{\parallel}$ and $I_{\perp}$ are emission intensities with parallel and perpendicular orientations of the detection polarizer with respect to the excitation polarizer which is held vertically. Correction was made for the polarization sensitivity of the detection monochromator using Azumi and McGlynn's procedure.[13]

All polarization spectra were measured near −165 °C in N_2-saturated 1-propanol. At this temperature, 1-propanol forms a stable and strain-free glass, although severe cracking does occur below −170 °C. Since it is important that rotational relaxation time of the emitting molecule be long compared with its emission lifetime, P was checked as a function of temperature and was found to be constant up to −135 °C. Usually emission was monitored at the luminescence maximum. In the case of $[Ir(P{=}P)_2]Cl$, however, extensive overlap between the 538-nm absorption band and the 545-nm emission band required that the polarization of the 538-nm band be measured by monitoring the red edge of emission. This introduced no error because the emission polarization was found invariant throughout its bandwidth. The accuracy of P is estimated to vary between ±10% at band maxima and ±50% in regions of low polarization and weak absorption.

Materials. The complexes were prepared from $IrCl(CO)(PPh_3)_2$ and $RhCl(CO)(PPh_3)_2$ and the free ligands (Strem Chemicals) according to Vaska and Catone's[14] procedure. Care was taken that handling and synthesis of the Ir(I) complexes were done in N_2-saturated solvents. 1-Propanol (Fisher) was used as received.

Results

Excitation spectra uncorrected for polarization induced by the emission monochromator and the calculated excitation polarization spectra are shown for $[Ir(P{=}P)_2]Cl$ and $[Rh(P{=}P)_2]Cl$ in Figures 1 and 2. Absorption between the two lowest energy bands in each spectrum was too weak to permit reliable measurements, so the polarizations are omitted in these regions. It is worth noting that the excitation spectra are also uncorrected for wavelength variations in lamp intensity and excitation monochromator transmission so that the excitation intensities bear little resemblance to absorption intensities, particularly below 400 nm. This is of no consequence in measuring P since all that is required is that the excitation remain constant for consecutive $I_{\parallel}$ and $I_{\perp}$ measurements. Low-temperature absorption and emission spectra for these complexes have been published.[11]

The first band for each complex is positively polarized with P ranging from 0.10 to 0.14. The differences among P for this band are close to the precision of the measurements and are not regarded as significant. An intense band with strong negative polarization (−0.24 to −0.30) comes next in each spectrum. Following this, a weak band, also negatively polarized, is resolved in $[Rh(P{=}P)_2]Cl$ and $[Ir(P{=}P)_2]Cl$ at ~370 and ~405 nm, respectively. This feature is not seen in $[Rh(P{-}P)_2]Cl$ or $[Ir(P{-}P)_2]Cl$, presumably because the

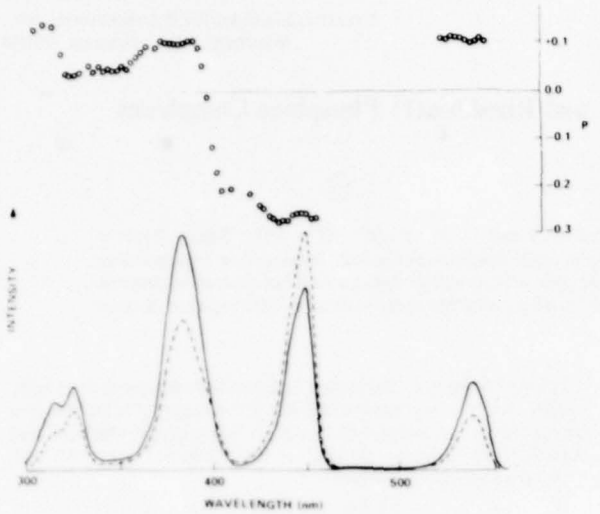

Figure 1. Polarized excitation spectra of $[Ir(P{=}P)_2]Cl$ in 1-propanol at −165 °C taken with $I_{\parallel}$ (—) and $I_{\perp}$ (- - -); calculated P values are shown by circles.

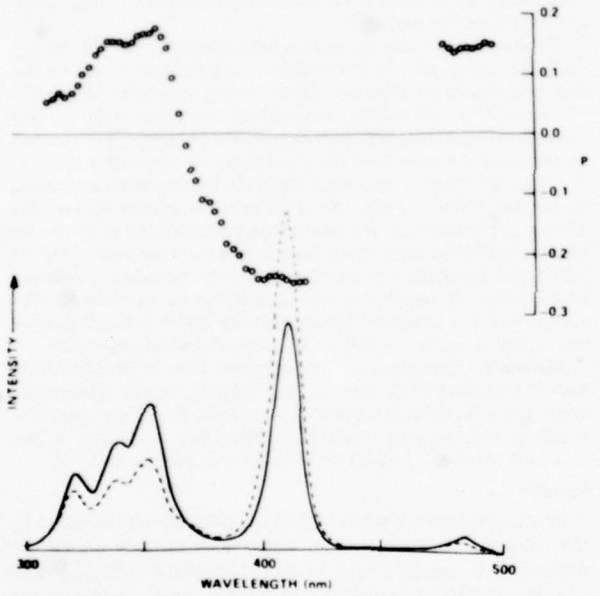

Figure 2. Polarized excitation spectra of $[Rh(P{=}P)_2]Cl$ in 1-propanol at −165 °C taken with $I_{\parallel}$ (—) and $I_{\perp}$ (- - -); calculated P values are shown by circles.

latter complexes show somewhat broadened absorptions, and this weak band is obscured by the adjacent intense band which has positive polarization. The polarization pattern of the three highest energy bands differ between the Rh and Ir complexes. In Ir, the sequence is positive, negative, positive with the middle band only attaining $P \sim 0$ because of the extensive overlap with the highest energy positive band. In $[Rh(P{-}P)_2]Cl$ the three bands are positively polarized, whereas in $[Rh(P{=}P)_2]Cl$ the highest energy band shows somewhat diminished polarization relative to the preceding two. Band positions and excitation polarizations measured at these maxima are collected in Table I.

Discussion

By proper averaging over all molecular orientations, it can be shown that photoselection of a random array of absorbing molecules leads to polarization limits of $-{}^1/_3 \leq P \leq +{}^1/_2$.[12] These limits occur when the absorbing and emitting oscillators

Table I. Summary of Assignments, Band Positions, and Polarizations in 1-Propanol at −165 °C

λ, nm	P	λ, nm	P	assignment $\leftarrow {}^1A_{1g}$	
$[Ir(P{=}P)_2]Cl$		$[Ir(P{-}P)_2]Cl$			
538	+0.10	527	+0.11	E_u ($^3A_{2u}$)	$a_{2u} \leftarrow a_{1g}$
449	−0.26	443	−0.30	A_{2u} ($^1A_{2u}$)	
~405[a]	−0.20				
383	+0.10	382	+0.07	E_u (^3E_u)	$a_{2u} \leftarrow e_g$
325	+0.03	~323[a]	0.00	A_{2u} (^3E_u)	
315	+0.14	319	+0.17	E_u (^1E_u)	
$[Rh(P{=}P)_2]Cl$		$[Rh(P{-}P)_2]Cl$			
483	+0.14	473	+0.12	E_u ($^3A_{2u}$)	$a_{2u} \leftarrow a_{1g}$
410	−0.25	412	−0.29	A_{2u} ($^1A_{2u}$)	
~370[a]	−0.10				
352	+0.17	351	+0.10	E_u (^1E_u)	$a_{2u} \leftarrow a_{1g}$
338	+0.15	338	+0.10		
321	+0.06	328	+0.10	(?)E_u (^1E_u)	$e_u \leftarrow a_{1g}$

[a] These bands are shoulders which are clearly resolved only in polarized spectra.

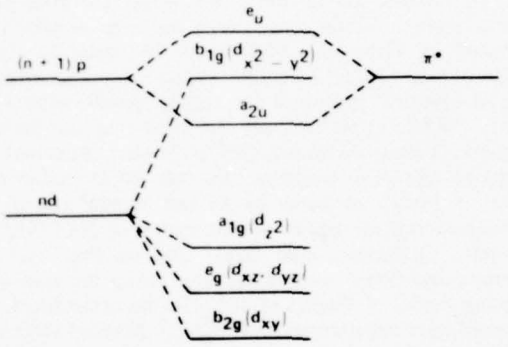

Figure 3. Partial molecular orbital diagram appropriate for iridium(I) and rhodium(I) phosphine complexes; D_{4h} symmetry is assumed.

are orthogonal and collinear, respectively. In the special case of in-plane absorption and emission, the maximum for P is reduced to $+{}^1/_7$. In practice these limits are rarely, if ever, realized. Overlapping bands of different polarizations, forbidden vibronic intensity within band envelopes, and excited state distortion as well as instrumental imperfections all serve to lower P from its theoretical maxima. In spite of these potential difficulties, experimental photoselection results frequently approximate theoretical limits well enough to be a reliable guide in assigning symmetries of excited states.

We assume that the d^8 bidentate phosphine complexes studied here have D_{4h} symmetry in the electronic ground state. As such, all symmetry-allowed electronic transitions can be classified as in-plane (x,y) or out-of-plane (z) polarized. P for the lowest energy band in each complex (Table I) closely approximates $+{}^1/_7$ and is, therefore, assumed to be in-plane polarized. If this band were out-of-plane, a much higher value for P could reasonably be expected because this band is well isolated from higher energy transitions (Figures 1 and 2). Further, the high degree of polarization of the second band (close to $-{}^1/_3$) rules out systematic errors or massive excited-state distortions which could lower P. The in-plane assignment is in accord with recent MCD results of Geoffroy et al.[10] which show this band to be degenerate. We conclude, therefore, that positive polarization corresponds to in-plane and negative polarization to out-of-plane transition moments.

A partial representation of molecular orbitals appropriate for these Ir(I) and Rh(I) complexes is shown in Figure 3. The metal d orbitals follow the ordering of Piepho et al.[3] for $Pt(CN)_4^{2-}$ and the a_{2u} and e_u ligand π^* orbitals conform to Gray and Ballhausen's[1] conclusions. This model predicts that the visible absorption of Ir(I) and Rh(I) bidentate phosphines

Table II. Double Group Theoretical States Generated from Lowest Energy $\pi^* \leftarrow$ d One-Electron Transitions

one-electron transition	double group (spin-orbit) excited states
$a_{2u} \leftarrow a_{1u}$	A_{2u} ($^1A_{2u}$), A_{1u} ($^3A_{2u}$), E_u ($^3A_{2u}$)
$a_{2u} \leftarrow e_g$	E_u (^1E_u), E_u (^3E_u), A_{1u} (^3E_u)
	A_{2u} (^3E_u), B_{1u} (^3E_u), B_{2u} (^3E_u)
$a_{2u} \leftarrow b_{2g}$	B_{1u} ($^1B_{1u}$), B_{2u} ($^3B_{1u}$), E_u ($^3B_{1u}$)
$e_u \leftarrow a_{1g}$	E_u (^1E_u), E_u (^3E_u), A_{1u} (^3E_u)
	A_{2u} (^3E_u), B_{1u} (^3E_u), B_{2u} (^3E_u)

should be dominated by allowed MLCT transitions of the type $a_{2u} \leftarrow$ d. The evidence has been summarized by others[10,11] that the lowest energy bands do fit the criteria for MLCT transitions.

The one-electron transitions $a_{2u} \leftarrow$ d give rise to three singlet and three triplet states of which two are optically accessible from the $^1A_{1g}$ ground state from spin and symmetry considerations ($^1E_u \leftarrow {}^1A_{1g}$ and $^1A_{2u} \leftarrow {}^1A_{1g}$). Spin–orbit coupling splits the triplets to yield a total of 12 states of which six are optically accessible (the E_u and A_{2u} double group states). The intensity of transitions to spin–orbit states of triplet origin will depend on the extent of singlet character acquired by the spin–orbit perturbation. For convenience, the double group states are listed in Table II.

The lowest energy band in each complex is positively polarized and is assigned to the in-plane transition E_u ($^3A_{2u}$) $\leftarrow {}^1A_{1g}$. As pointed out by Geoffroy et al.,[10] this band is stronger in Ir(I) than Rh(I) complexes which is consistent with the increase in spin–orbit coupling. The intense, negatively polarized second band is assigned to the out-of-plane A_{2u} ($^1A_{2u}$) $\leftarrow {}^1A_{1g}$. The intensities and polarizations of these two bands are consistent with the ordering of Piepho et al. for metal d orbitals which places a_{1g} as the highest occupied orbital. On the other hand, Interrante and Messmer's[6] calculation on $Pt(CN)_4^{2-}$, which predicts b_{2g} to be the highest occupied d orbital, leads to difficulties. If b_{2g} is highest, the second band could only arise from the A_{2u} component of ^3E_u ($a_{2u} \leftarrow e_g$). However, this interpretation requires that, at least in the case of Rh(I) complexes, the E_u component of ^3E_u ($a_{2u} \leftarrow e_g$) lie in the same spectral region. This is not observed in the spectra, and we conclude that the metal d-orbital ordering of Piepho et al.[3] is appropriate for these iridium(I) and rhodium(I) phosphines.

A previously unreported weak band with negative polarization is resolved as a shoulder near 405 nm in $[Ir(P{=}P)_2]Cl$ and 370 nm in $[Rh(P{=}P)_2]Cl$. The origin of the feature is uncertain. It possibly is a vibronic transition associated with A_{2u} ($^1A_{2u}$) $\leftarrow {}^1A_{1g}$ since the separation of these bands is $\sim$2600 cm^{-1} in both complexes.

Following Geoffroy et al.[10] the 383-, 325-, and 315-nm bands in $[Ir(P{=}P)_2]Cl$ are assigned to E_u (^3E_u) $\leftarrow {}^1A_{1g}$, A_{2u} (^3E_u) $\leftarrow {}^1A_{1g}$, and E_u (^1E_u) $\leftarrow {}^1A_{1g}$, respectively. All of these originate from $a_{2u} \leftarrow e_g$. This is in agreement with the polarization spectrum which shows the 325-nm band to be A_{2u}, although it strongly overlaps the adjacent E_u band. *P* for the analogous transition in $[Ir(P{-}P)_2]Cl$ becomes slightly negative (–0.02) near its maximum. Semiempirical calculations by Geoffroy et al.[10] show that the various E_u and A_{2u} states are thoroughly mixed so that absorption intensities among these transitions should be roughly the same. This expectation is realized in low-temperature absorption spectra.[11]

The situation in $Rh(P{=}P)_2Cl$ is less clear. *P* values for the 352- and 338-nm bands clearly indicate that they are E_u in character, whereas the 321-nm band has somewhat diminished positive polarization. The corresponding transitions in $[Rh(P{-}P)_2]Cl$ all show $P = 0.10$. It appears that none of these bands can be clearly associated with the A_{2u} component of ^3E_u ($a_{2u} \leftarrow e_g$). This, perhaps, is not too surprising in view of calculations on $[Rh(P{=}P)_2]Cl$ which predict the intensities of transitions to states of triplet origin should be more than a factor of 10 less intense than transitions to states of singlet origin.[10] The low-temperature absorption spectra show the intensities of these bands (321, 338, 352, and 410 nm) to vary less than a factor of 2.[11] It seems certain that E_u (^1E_u) $\leftarrow {}^1A_{1g}$ ($a_{2u} \leftarrow e_g$) must lie in this region and perhaps also E_u (^1E_u) $\leftarrow {}^1A_{1g}$ ($e_u \leftarrow a_{1g}$), but detailed assignments must await a more refined theoretical model than presently available.

Acknowledgment. We thank the Air Force Office of Scientific Research for support of this work under Contract No. F49620-77-C-0015.

Registry No. $[Ir(P{=}P)_2]Cl$, 36390-37-1; $[Ir(P{-}P)_2]Cl$, 15390-38-2; $[Rh(P{=}P)_2]Cl$, 22754-44-5; $[Rh(P{-}P)_2]Cl$, 15043-47-7.

References and Notes

(1) H. B. Gray and C. J. Ballhausen, *J. Am. Chem. Soc.*, **85**, 260 (1963).
(2) W. R. Mason, III, and H. B. Gray, *J. Am. Chem. Soc.*, **90**, 5721 (1968).
(3) S. B. Piepho, P. N. Schatz, and A. J. McCaffery, *J. Am. Chem. Soc.*, **91**, 5994 (1969).
(4) C. D. Cowman, C. J. Ballhausen, and H. B. Gray, *J. Am. Chem. Soc.*, **95**, 7873 (1973).
(5) H. Isci and W. R. Mason, *Inorg. Chem.*, **14**, 905, 913 (1975).
(6) L. V. Interrante and R. P. Messmer, *Chem. Phys. Lett.*, **26**, 225 (1974).
(7) D. G. Marsh and J. S. Miller, *Inorg. Chem.*, **15**, 720 (1976).
(8) R. Brady, B. R. Flynn, G. L. Geoffroy, H. B. Gray, J. Peone, Jr., and L. Vaska, *Inorg. Chem.*, **15**, 1485 (1976).
(9) C. D. Cowman and H. B. Gray, *Inorg. Chem.*, **15**, 2823 (1976).
(10) G. L. Geoffroy, H. Isci, J. Litrenti, and W. R. Mason, *Inorg. Chem.*, **16**, 1950 (1977).
(11) G. L. Geoffroy, M. S. Wrighton, G. S. Hammond, and H. B. Gray, *J. Am. Chem. Soc.*, **96**, 3105 (1974).
(12) A. C. Albrecht, *J. Mol. Spectrosc.*, **6**, 84 (1961).
(13) T. Azumi and S. P. McGlynn, *J. Chem. Phys.*, **37**, 2413 (1962).
(14) L. Vaska and D. L. Catone, *J. Am. Chem. Soc.*, **88**, 5324 (1966).

APPENDIX B

RADIATIONLESS DECAY IN RHODIUM(I) AND IRIDIUM(I) COMPLEXES: POLARIZATION AND SOLVENT RELAXATION STUDIES

RADIATIONLESS DECAY IN RHODIUM(I) AND IRIDIUM(I) COMPLEXES: POLARIZATION AND SOLVENT RELAXATION STUDIES

Leonard J. Andrews
GTE Laboratories Incorporated
40 Sylvan Road
Waltham, Massachusetts 02154

ABSTRACT

Radiationless decay in the complex Ir [cis-1,2-bis(diphenylphosphino ethylene] chloride and its Rh(I) analog have been characterized in 1-propanol and glycerol. Decay in the Rh(I) complex and, to a lesser extent, in the Ir(I) complex is controlled by solvent rigidity and not by temperature. Excitation polarization and wavelength dependent emission decay studies show that neither solute nor solvent rotational relaxation play a role in the decay.

INTRODUCTION

Recently, several Ir(I) and Rh(I) bidentate phosphine complexes have been added to the rapidly expanding list of photoluminescent transition metal complexes.[1] These complexes incorporate the π-acid ligand cis-1,2-bis(diphenylphosphino)ethylene (P=P) or its ethane analog and adopt the square planar configuration common in d^8 systems. Their luminescence has been characterized as metal-to-ligand charge transfer (MLCT) and assigned to the E_u component of a $^3A_{2u}$ state which gains intensity through spin-orbit coupling. This assignment has been corroborated by magnetic circular dichroism[2] and polarized excitation spectra.[3] Also, radiative lifetimes lie in the range 10^{-4}s to 10^{-5}s which is consistent with the partially forbidden character of the emission.

An interesting aspect of the $M(P=P)_2Cl$ [M = Ir(I), Rh(I)] complexes is the extreme temperature dependence of the emission quantum yield. While $M(P=P)_2Cl$ emit in glassy organic solvents at 77°K with yields which approach unity, they are totally nonemissive in degassed fluid solution at ambient temperature.[1] Since it has long been appreciated that solvent viscosity can exert an important influence on molecular spectral and photophysical properties, we have investigated the temperature dependences of the emission for these complexes in the glass-forming solvents 1-propanol and glycerol. The aims are to separate the effects of temperature and viscosity on radiationless decay and to use luminescence as a probe of solute-solvent interaction in the temperature ranges where emission becomes negligible.

EXPERIMENTAL

Steady State Measurements — Emission spectra, intensities and excitation polarization were measured on a fluorimeter consisting of a 150W Xe arc, a 0.25m Jarrel Ash 82-410 excitation monochrometer, a 0.5m Perkin Elmer E1 emission monochrometer, an RCA C31034 photomultiplier and a Keithley 411 micro-microammeter. Excitation and emission beams were oriented at right angles. Samples were contained in a 0.5 cm Pyrex tube which was enclosed in a quartz dewar and cooled with N_2 gas. The temperature of the flowing N_2 was sensed by a Pt resistance thermometer which controlled a heater in the gas flow through a feedback circuit. An iron-constantan thermocouple was immersed directly in the sample. This apparatus was modified for polarization measurements as previously described.[3] Emission spectra are uncorrected for detector and monochrometer distortion. Emission intensities were assumed proportional to the product of peak height and bandwidth at half maximum.

Lifetime Measurements — An N_2 laser pumped dye laser (Stilbene 3, 5 ns pulse width, 1Å resolution) was used to excit $M(P{=}P)_2Cl$ complexes in their second absorption band (418 nm for Rh(I) and 450 nm for Ir(I)). Sample temperature was controlled and monitored with an arrangement identical to that used in the fluorimeter. Decay curves were recovered using a P.A.R. Model 162 boxcar integrator. Decay of total emission was measured using a glass cutoff filter (Schott GG420 or OG530) and a C31034A RCA photomultiplier. This tube is equipped with a GaAs photocathode and has a nearly flat energy response over the spectral range of $M(P{=}P)_2Cl$ luminescence. Since a spectrally flat response might be important for some decay measurements, results were checked with an S-20 photomultiplier (RCA 7265) and were found to be identical with the GaAs tube data. Portions of the emission spectrum for $Rh(P{=}P)_2Cl$ were isolated for lifetime measurements using interference filters (Baird-Atomic, 548 ± 2 nm and 678 ± 7 nm, the deviations indicate the width at 50% peak transmission).

Time Resolved Spectra — Time resolved spectra of $Rh(P{=}P)_2Cl$ emission were recorded using the 0.25m Jarrel Ash equipped with an RCA 4832 photomultiplier and dye laser excitation at 418 nm. The RC time constant of the detection circuit was approximately 350 ns with a 1 kohm photomultiplier load and the sampling gate of the model 162 boxcar was set at 500 ns.

Materials — The Ir(I) and Rh(I) complexes were prepared using Vaska and Catone's[4] method. Care was taken to exclude O_2 during synthesis and storage of $Ir(P{=}P)_2Cl$. 1-propanol (Fisher) and glycerol (Baker) were used as received. All sample solutions were saturated with N_2 and complex concentration was approximately 1×10^{-4}M, except for the time resolved spectral measurements which were recorded with 3×10^{-4}M solutions.

RESULTS

$Ir(P{=}P)_2Cl$ — The first absorption band and emission spectrum of $Ir(P{=}P)_2Cl$ in 1-propanol glass are shown in Figure B-1. They agree well with previously published spectra in EPA at 77°K.[1] To a good approximation these spectra are mirror images with a 300 cm^{-1} Stokes shift at 85°K and an emission halfwidth at half maximum (HWHM) of 250 cm^{-1}. Between 85° and 165°K in 1-propanol, the emission undergoes a small red shift (approx. 50 cm^{-1}) and almost no change in bandwidth.

The temperature dependences of the emission lifetime (τ) in 1-propanol and glycerol are shown in Figure B-2. For these measurements total emission

was detected. At all temperatures in both solvents no deviation from exponential decay was detected over the three 1/e lifetimes emission could be monitored. At 85°K, the lifetime of $Ir(P=P)_2Cl$ in 1-propanol was 9.4 μs which can be compared with 8.2 μs reported for this complex in EPA at 77°K.[1]

Figure B-2 shows that the temperature dependence of the emission lifetime is complex in these glass forming alcohols. Below 125°K, the data in 1-propanol and glycerol are identical with τ sharply increasing with no maximum evident down to 85°K. In 1-propanol, an inflection point occurs at 125°K signaling the activation of a second decay channel. This process rapidly dominates radiative decay so that above 170°K emission is negligible. In glycerol, the activation of this second process is shifted 100°K to higher temperatures, so that emission becomes negligible above 270°K in this solvent.

Relative total intensity measurements were also made in each solvent. Measurements could be made down to 105°K in 1-propanol and 200°K in glycerol. Below these temperatures extensive solvent cracking made accurate relative intensity measurements impossible. The maximum intensities (lowest temperature points) were arbitrarily normalized to lie on the τ vs. T curves (Figure B-2) and, plotted in this manner, it is seen that lifetimes and intensities change with temperature in parallel fashion in both solvents.

Also shown in Figure B-2 are the temperature dependences of the excitation polarization (P). For these measurements, the second absorption band at 449 nm was pumped and emission was monitored at the 545 maximum. The transition moment for the pump band is perpendicular to the IrP_4 plane ($A_{2u} \leftarrow A_{1g}$) and the emission moment lies in-plane ($E_u \rightarrow A_{1g}$), consequently P is a large negative number (-0.26) close to the theoretical limit of -1/3.[3] P was found to be the same in each solvent and invariant over the temperature ranges 105° to 155°K in 1-propanol and 210° to 265°K in glycerol. The lower temperature limit was determined by solvent cracking and the upper limit by the sensitivity of the photoselection apparatus.

$Rh(P=P)_2Cl$ — Figure B-3 shows the first absorption band and emission spectra of $Rh(P=P)_2Cl$ in 1-propanol glass. In agreement with the previously reported spectrum[1] there is a lack of mirror symmetry and a large Stokes shift (4000 cm^{-1} at 94°K). Further, the emission maximum undergoes a red shift of 540 cm^{-1} (from 598 nm to 618 nm) over the range 85° to 170°K, while the HWHM increases from 975 to 1100 cm^{-1} over the same temperature range.

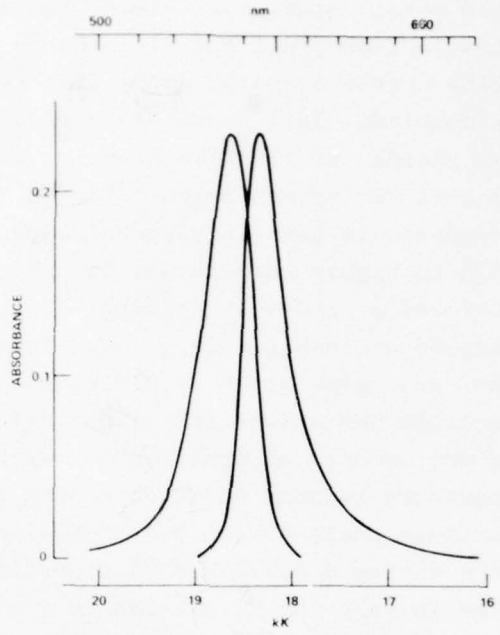

Figure B-1. Absorption (1.2×10^{-4}M, ℓ = 1 cm, 165°) and Emission (9.4×10^{-6}M, 117° K) of $I(P=P)_2Cl$ in 1-Propanol.

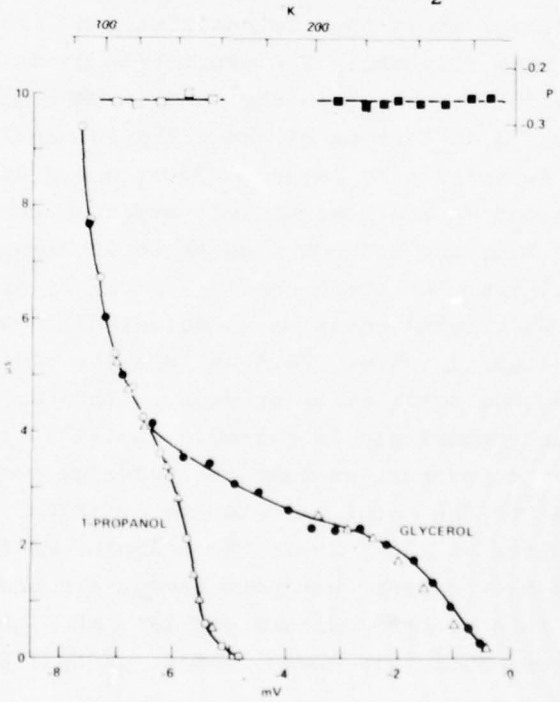

Figure B-2. Ir(P=P). Temperature Dependence of Emission Lifetime in 1-Propanol (○) and glycerol (●) and Relative Emission Intensity (△). Excitation polarization in 1-propanol (□) and glycerol (■).

Figure B-4 shows the total emission lifetime, relative total intensity and emission polarization in 1-propanol and glycerol as a function of temperature. The lifetime curves are distinctly different from those observed with the Ir(I) complex. In 1-propanol, τ rises sharply from near zero at 150°K, attains a plateau at 120°K and remains constant to 85°K. The average τ in the plateau region was measured to be 28.5 ± 2 μs. A similar temperature dependence is seen in glycerol except that the τ vs. T curve is translated 100°K to higher temperature and the low temperature limiting τ is nearly achieved at 200°K in glycerol (25 μs).

Using the GaAs equipped photomultiplier, τ was found to be exponential below 120°K in 1-propanol and below 210°K in glycerol. Above these temperature, small but reproducible deviations from exponentiality occur in which the apparent decay constant becomes slightly longer with time. The lifetime in these high temperature regions shown in Figure B-4 represent approximations in which these small deviations from linearity were ignored and the best fit over the entire decay was used to estimate τ. This procedure seems justified in that the variations in τ at different temperatures always greatly exceeded the variations of τ at constant temperature.

The temperature dependence of the relative total emission intensity is also shown in Figure B-4. Normalization of the highest intensity points to lie on the τ vs. T curves shows that intensities and lifetimes change in parallel fashion in both solvents. The excitation polarization for the second absorption band ($A_{2u} \leftarrow A_{1g}$) is the same in both solvents (-0.23) and is invariant up to 137°K in 1-propanol and 237°K in glycerol.

The wavelength dependence of emission decay was studied for $Rh(P{=}P)_2Cl$ in 1-propanol. Portions of the luminescence spectrum centered at 548 and 678 nm (the emission blue and red edges as shown in Figure B-3) were isolated with interference filters. As noted earlier, decay is exponential below 120°K in 1-propanol when total emission is detected. However, at 82°K, the blue edge decay is slightly faster (26.5 μs) and the red edge decay slightly slower (30.9 μs) than the total emission decay. This anomalous behavior is exacerbated as the temperature is raised. At 117°K, the blue edge decay shows a distinct fast component, whereas the red edge decay remains nearly exponential and equal to the total emission decay (Figure B-5). This description also applies at 130°K (near the midpoint of the τ vs. temperature curve in Figure B-4) except that both decays are accelerated relative to the 117°K data. This general pattern persists at higher temperatures until emission becomes negligible above approximately 150°K.

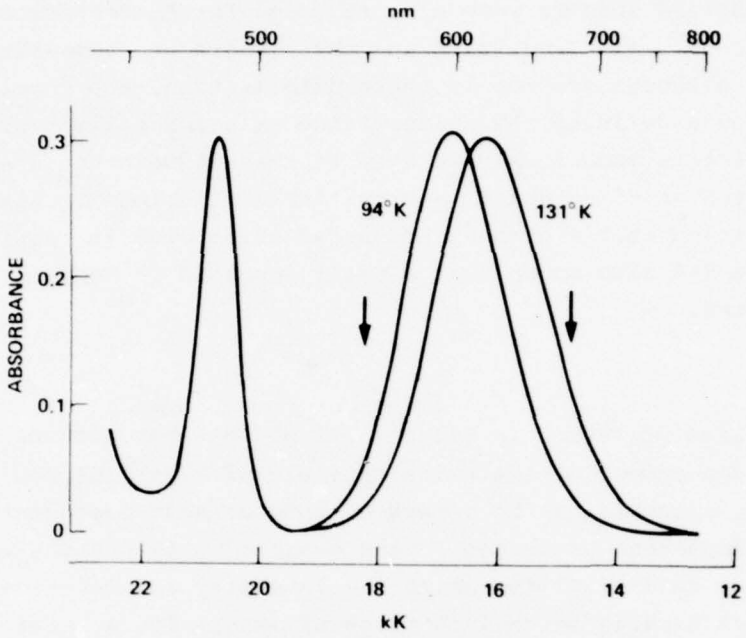

Figure B-3. Absorption (1.0×10^{-3}, ℓ = 1 cm, 137°K) and Emission (1.0×10^{-4}M) of $Rh(P{=}P)_2Cl$ in 1-Propanol. Arrows refer to the positions of maximum transmission of interference filters used in wavelength dependent decay studies (F gure B-5).

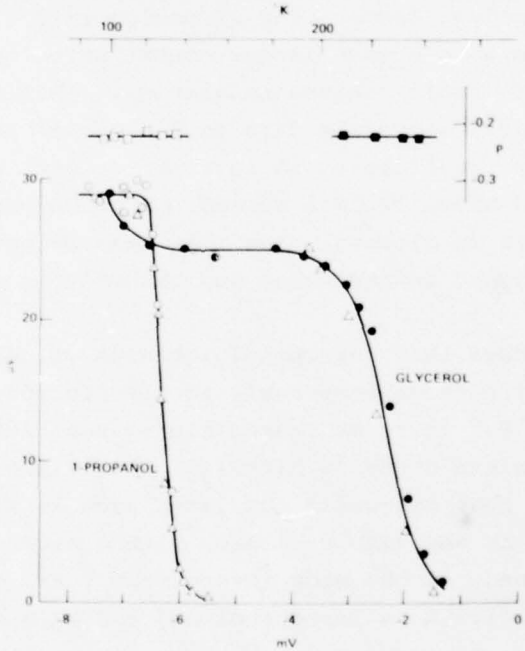

Figure B-4. $Rh(P{=}P)_2Cl$. Temperature Dependence of Emission Lifetime in 1-Propanol (○) and Glycerol (●) and Relative Emission Intensity (△). Excitation polarization in 1-propanol (□) and glycerol (■).

Time-resolved spectra were also recorded for $Rh(P{=}P)_2Cl$ emission in 1-propanol at 94°, 114° and 124°K and the results are summarized in Figure B-6. Although scatter in these data is high, the results at 114° and 124°K show a definite red shift of the emission maximum with time. At 94°K this shift is much less, but even at this temperature a slight shift can be detected at 85 μs delay (approx. three lifetimes). Also note that the peak position at t = o undergoes a red shift with increasing temperature. Figure B-6 also shows that a small decrease in bandwidth with time can be detected.

DISCUSSION

The results presented in Figures B-2 and B-4 demonstrate that the apparent temperature dependence of the emission yield of $M(P{=}P)_2Cl$ complexes in glass-forming alcohols can be separated into solvent-dependent and temperature dependent processes. This separation is particularly striking in the case of $Rh(P{=}P)_2Cl$ for which the intensity and lifetime data in 1-propanol are closely matched in glycerol except for a shift of approx. 100°K to higher temperatures. This shows that the variation of yield for $Rh(P{=}P)_2Cl$ emission is nearly temperature independent and is controlled by a parameter specifically associated with solvent. From the parallel behavior of intensity and lifetime, the yield variation is attributable to changes in radiationless decay. The situation in $Ir(P{=}P)_2Cl$ is more complex in that there is a much larger contribution of a temperature dependent process to radiationless relaxation. This temperature dependence is evident below 120°K where the data in 1-propanol and glycerol are identical. At this temperature, an inflection point occurs in the 1-propanol curve, and above 120°K a second radiationless decay must become activated. The data in glycerol show that this second process is extended roughly 100°K to higher temperatures and therefore must be associated with solvent.

Since it is known that 1-propanol achieves values for viscosity and dielectric relaxation rates comparable to glycerol only at temperatures lower by 80° to 90°K,[5] it seems reasonable to associate the solvent dependent radiationless decay in $M(P{=}P)_2Cl$ with viscoelastic properties. This does not mean that molecular constants such as luminescence lifetime need be correlated in any simple fashion with a macroscopic parameter such as viscosity. Indeed, at the midpoints of the τ vs. temperature curves for $Rh(P{=}P)_2Cl$ (approx. 128°K in 1-propanol and 228°K in glycerol) the viscosity

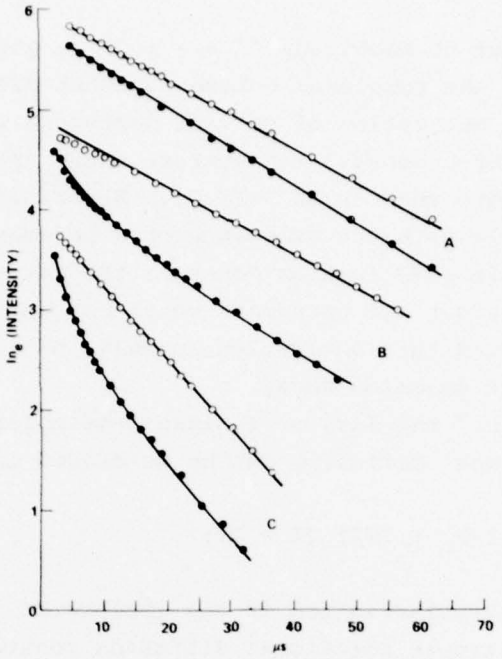

Figure B-5. Plots of ℓn_e (Intensity) vs. Time for $Rh(P=P)_2Cl$ Decay in 1-Propanol Monitoring 548 nm (●) and 678 nm (○) at 92°K (A), 117°K (B) and 130°K (C). Solid lines are calculated fits using modified Lessing model (see text).

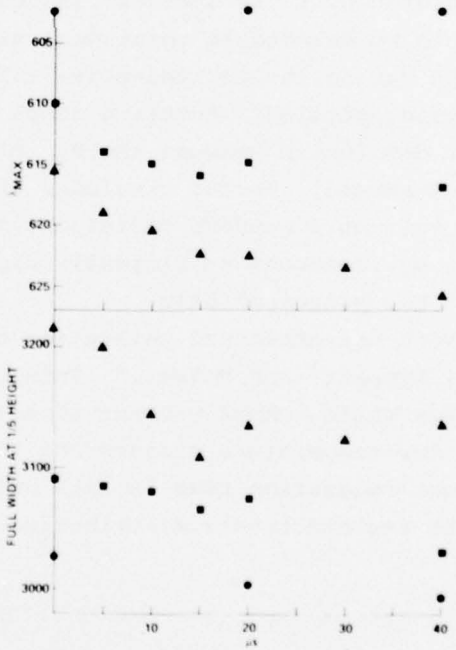

Figure B-6. Upper: Plots of λ_{max} for the Time Resolved Emission of 3×10^{-4}M $Rh(P=P)_2Cl$ in 1-Propanol at 94°K (●), 114°K (■) and 124°K (▲); Lower: Plots of the Full Width at 1/5 Peak Height of the Time Resolved Emission at the Same Temperatures. The bandwidth data at 114°K was reduced by 75 cm^{-1} for clarity in the figure.

differs by about an order of magnitude (1.4×10^5P in glycerol and 2×10^4P in 1-propanol).[5] Also, the complexes behave somewhat differently in the same solvent, i.e., the activation of solvent dependent radiationless decay in $Ir(P{=}P)_2Cl$ occurs over a broader temperature range and is shifted approx. 20°K to higher temperature than in $Rh(P{=}P)_2Cl$. Nevertheless, the results overall appear compatible with the existence of a parameter which we call solvent rigidity which in some fashion controls the activation of radiationless decay. We now consider two phenomena which can sharpen our preception of molecular motion during this activation, namely, excitation polarization and wavelength dependent emission decay.

According to Perrin,[6] the loss of luminescence polarization of spherical molecules due to rotational diffusion can be described as follows:

$$1/P - 1/3 = (1/P_o - 1/3)\ (1 - D\tau) \qquad (1)$$

where P_o is the limiting polarization in the absence of rotation, D is the viscosity dependent isotropic rotational diffusion constant, and τ is the excited-state lifetime. Since the limiting polarization P_o is observed for both $M(P{=}P)_2Cl$ complexes in each solvent at all temperatures, it follows that $D << \tau^{-1}$ under all conditions studied here, i.e., the rotational relaxation is not correlated with the increase in radiationless decay. To be more precise, there is no detectable rotational diffusion about axes containing the MP_4 plane during the excited-state lifetime, since only such rotational will depolarize emission. Rotation about the axis perpendicular to the MP_4 plane cannot depolarize because the D_{4h} microsymmetry makes the in-plane transitions degenerate. We can conclude, therefore, that over the temperature range that solvent dependent radiationless decay is activated, the complexes reside in environments sufficiently rigid to inhibit rotation about at least two principal axis.

The effect of solvent orientational relaxation on luminescence spectra was first recognized by Lippert[7] and Mataga.[8] This effect was used to rationalize the frequency shift commonly observed between molecular fluorescence in rigid, low-temperature glasses and that seen in fluid solution. If the solvent relaxation time is fast compared with the excited-state lifetime, then the new electronic distribution created on excitation

will be accommodated optimally by the surrounding solvation sphere and a potential energy minimum will be achieved during the excited-state lifetime. On the other hand, if solvent relaxation is slow compared with the excited-state lifetime, as in a rigid glass, then in general, the optimum solute-solvent configuration cannot be realized and an emission blue shift results. A blue shift is the normal observation because solute-solvent interactions are usually stronger when the solute is excited, although in principle a red shift could occur. In recent years, beginning with Ware,[9] although earlier attempts were made by Bakhshiev,[10] the dynamics of solvent relaxation have been investigated by choosing experimentally the interesting condition of solvent relaxation times similar to excited-state lifetimes. For these studies, solutes which develop large dipole moments in their excited states and are dissolved in polar solvents are usually chosen. This is precisely the case encountered here, i.e., a polar metal-to-ligand charge transfer excited state in an alcoholic solvent (however, vide infra). We attribute temperature induced shifts in emission spectra (Figure B-2), nonexponential wavelength decay kinetics (Figure B-5) and time-dependent emission spectra (Figure B-6), to orientational relaxation of dipolar solvent molecules during the excited state lifetime. We now proceed to extract solvent relaxation rates from lifetime data to establish whether or not a correlation exists between this relaxation and solvent dependent radiationless decay in $Rh(P{=}P)_2Cl$. To do this, the model described recently by Lessing, et al.[11,12] will be used.

The Lessing approach is an heuristic formulation which rests on the following postulates: (1) the excited solute is surrounded by m solvent molecules which relax independently and exponentially with rate k_s, (2) if $\Delta\nu_s$ is the hypothetical shift (relaxation width) in the luminescence spectrum between totally relaxed solute-solvent configurations and completely unrelaxed configurations (the initially produced Frank-Condon states which emit at ν_o), then relaxation of each solvent molecule produces a spectral shift $\Delta\nu_s/m$, (3) the quantum yield of luminescence as well as band shape are independent of the state of solvent relaxation. These postulates lead to the following set of equations:

$$\dot{N}(0,t) = -(k_f + mk_s)\, N(0,t)$$

$$\dot{N}(1,t) = -[k_f + (m-1)]\, N(1,t) + mk_s\, ((0,t)$$

$$\vdots$$

$$\dot{N}(m,t) = -k_f\, N(m,t) + k_s\, N(m-1,t) \qquad (2)$$

where N(i,t) is the time-dependent population of solute molecules surrounded by i relaxed solvent molecules, and $k_f = 1/\tau$ where τ is the experimental excited-state lifetime. Summing Eq. (2), we obtain Eq. (3).

$$\dot{\eta}(t) = k_f \, \eta(t)$$

$$\eta(t) = \sum_{i=o}^{m} N(i,t) \tag{3}$$

This result implies that if emission from all populations of solute molecules is detected with equal probability then this total emission must decay exponentially if the yield is independent of solvent relaxation. Thus the assumption of invariant yield can be easily checked experimentally with a detector which is spectrally flat throughout the emission band. Finally, we assume that the intensity of the emission band is governed by a Gaussian distribution, because the steady state $Rh(P{=}P)_2Cl$ emission is well described as Gaussian. This leads to the following expression for $I(\nu,t)$ which is the time dependent intensity at wavenumber ν (photons/cm^3 s cm^{-1}).

$$I(\nu,t) = \frac{k_r}{\Delta\nu(\pi/\ell n2)^{1/2}} \sum_{i=o}^{m} N(i,t)$$

$$\times \exp\left\{-[\nu-(\nu_o - i\,\Delta\nu_s/m)]^2 \, \ell n2/\Delta\nu^2\right\} \tag{4}$$

where k_r is the radiative decay rate, $\Delta\nu(\pi/\ell n2)^{1/2}$ is a normalization factor insuring that the integrated emission spectrum of each population N(i,t) is unity and $\Delta\nu$ is the HWHM.

In our application of Eq. (4), m is chosen to be 5 because of Lessing's[12] recent result that the fitted parameters for the decay of 4-dimethylamino-4'-nitrostilbene in dibutyl ether are independent of m for $m \geq 4$. The set of Eqs. (2) were first solved using the Runge-Kutta numerical integration procedure and then $I(\nu,t)$ was calculated. Values for k_f are fixed by the total emission decay constant and k_s is a fitted parameter. For the spectral parameters, ν is the observation wavelength, ν_o is taken to be the emission maximum at 85°K (16,720 cm^{-1}), $\Delta\nu$ is the observed steady-state bandwidth at the temperature of the pulsed experiment, and $\Delta\nu_s$, the relaxation width, is the second fitted parameter.

It was possible to fit the small variations in emission decay constant at 92°K with this model by choosing $k_s = 2 \times 10^4$ s^{-1} and $\Delta\nu_s = 100$ cm^{-1}. The calculated values of 27.3 μs (548 nm) and 31.4 μs (678 nm) agree within the experimental uncertainty with the observed decay constants of 26.5 and 30.9 μs. However, at higher temperatures, where the spectroscopic effects of solvent relaxation become more pronounced, it was not possible to choose a set of kinetic and spectroscopic parameters which could simultaneously reproduce the blue and red edge decay. Acceptable fits could be obtained only by modifying Lessing's model in two respects. First, the assumption that each population N(i,t) of solvated $Rh(P{=}P)_2^+$ ions at a given temperature has the same emission spectrum except for a shift $\Delta\nu_s/m$ was abandoned. Instead it was assumed that the emission bandwidth decreases with solvent relaxation. This spectral narrowing seems reasonable when one considers that the excited state is created with an inappropriate solvation sphere which relaxes to some optimum energy configuration. Such a process would seem to reduce the range of solvation sites experienced by the complex and it is these which are ultimately responsible for the inhomogeneous width of the transition. Spectral narrowing was incorporated into Eq. (4) by substituting $\Delta\nu' = \Delta\nu - \Delta\nu_s/m$, i.e., the emission halfwidth was assumed to decrease by the amount of the relaxation shift. Without this change, parameters which led to acceptable fits at 548 nm would predict excessive initial intensity growths at 678 nm which were not observed. At best, only a slight growth could be detected at the red edge under any conditions.

The second modification is that ν_o, the position of the emission peak at t = 0, is temperature dependent. This was required by the result that the calculated fits are quite sensitive to the relaxation width, $\Delta\nu_s$, and the best fits at all temperatures are obtained with $\Delta\nu_s = 100 - 120$ cm^{-1} (Table B-1). This means that if ν_o is chosen to be 16,720 cm^{-1} (the position of the steady state 85°K emission maximum), then even complete relaxation cannot reproduce the observed steady state emission maximum at 117°K (16,350 cm^{-1}) or 130°K (16,200 cm^{-1}). In order to be consistent with the steady-state results, it is necessary to assume ν_o undergoes a red shift with increasing temperature. Parenthetically, the calculated fits are not especially sensitive to the precise value of ν_o within the range 16,800 to 16,200 cm^{-1}.

The results of time-resolved spectra summarized in Figure B-6 support these modifications. The peak positions of spectra taken at t = 0 (i.e., the initial 500 ns) show a pronounced red shift with increasing temperature.

TABLE B-1

PARAMETERS USED FOR FITTING 678 AND 548 nm DECAY CURVES SHOWN IN FIGURE 5

T	k_f*	$\Delta\nu$ (HWHM)**	$\Delta\nu_s$	k_s
130°K	7.24×10^4 s^{-1}	1080 cm^{-1}	120 cm^{-1}	2.5×10^5 s^{-1}
117°K	3.33×10^4 s^{-1}	1050 cm^{-1}	120 cm^{-1}	1.0×10^5 s^{-1}
92°K	3.46×10^4 s^{-1}	1000 cm^{-1}	100 cm^{-1}	0.2×10^5 s^{-1}

*Decay constant measured by monitoring total emission.
**Value of HWHM of steady-state emission band.

Further, the time dependence of ν_{max} at 114° and 124°K do not appear to permit extrapolation to the ν_o measured at 94°K. Very similar observations have been reported for the time-resolved fluorescence spectra of 4-aminophthalimide in hydroxylic solvents.[9] In this case the temperature dependence of ν_o was attributed to an "ultrafast" exciplex formation unresolvable on a nanosecond time scale which was followed by "normal" solvent relaxation. It is possible that a similar mechanism is responsible for the ν_o shift observed here. Figure B-6 also shows that the emission bandwidth undergoes a slight but detectable decrease with time, whereas the Lessing model requires that an increase must occur during relaxation. It should be stressed that the observed spectral narrowing is a small effect. The data shown in Figure B-6 are the full width at one-fifth peak height. The corrected bandwidths incorporated into Eq. (4) probably overcompensate for this effect, but no attempt was made to optimize the extent of spectral narrowing in the model.

The solid line fits to the 548 and 678 nm decay of $Rh(P{=}P)_2Cl$ in 1-propanol shown in Figure B-5 were calculated using the parameters listed in Table B-1. Although the evident agreement between experiment and the modified Lessing model does not prove that solvent relaxation is responsible for wavelength dependent decay, it is difficult to understand these results in terms of an intramolecular model, i.e., of distorted complexes. Consider the data at 117°K where the decay of total emission is strictly exponential and equal to the 85°K decay constant. Figure B-5 shows that wavelength dependent decay effects are pronounced even though at this temperature τ lies in the plateau region of Figure B-5. If wavelength dependent decays were due to various populations of distorted complexes, it would be remarkable that their emission quantum yields are identical as implied by exponential decay of total emission. It seems far more probable that

solvent relaxation causes the behavior shown in Figure B-5, since solvent effects would be expected to exert a much smaller effect on emission yield than molecular distortion as well as provide a sensible interpretation for all the results outlined earlier.

In Table B-1 the solvent relaxation time, k_s^{-1}, range from 4 to 50 μs, and it is of interest to compare these values with those calculated from the Debye-Stokes-Einstein relation [Eq. (5)].[13]

$$k_s^{-1} = \tau_s = 3\ \eta v/kT \qquad (5)$$

At 130°K, the extrapolated value for the viscosity is 1.2×10^4 Poise[5] and, assuming a molecular volume of $v = 104 \times 10^{-24}$ cm^3 (calculated from the 300°K density of 1-propanol and an assumed 20% solvent contraction), τ_s is found to be 200 μs. Similarly at 117°K, $\eta = 3.1 \times 10^6$ Poise[5] and τ_s is 60 ms. Although some error exists in the extrapolated values for η, it seems clear that the Debye-Stokes-Einstein relaxation times are much longer than those calculated from spectral effects. One possible explanation for this disparity is that the molecular motion required for spectral effects is much smaller than that required for a macroscopic viscoelastic property. For example, a twist of an hydroxyl group may be important spectrally, whereas rotation of the alcohol as a whole or even cooperative effects among several solvent molecules is probably required to explain viscous flow. This would lead to much smaller effective molecular volumes for spectral effects than that calculated from a simple space filling model as done above, with a concomitant decrease in τ_s.

CONCLUSIONS

The description which emerges from this study is that activation of radiationless decay in $Rh(P{=}P)_2Cl$ in hydroxylic solvents is nearly exclusively controlled by solvent rigidity. Polarization results show that during activation the complex does not freely rotate. On the other hand, solvent relaxation does occur during activation, but data taken at 117°K shows that solvent relaxation does not promote radiationless decay and is only cotemporaneous with it.

The effect of solvent rigidity on luminescence yields has been noted for metal complexes incorporating Ru(II),[14,15] Rh(III)[16] and Cr(III).[17] In all cases, a satisfactory explanation is lacking. There have also been recent reports of temperature dependent changes in the nature of the

emitting electronic state which have been attributed to viscoelastic properties of the solvent.[18,19] In these cases, a potential energy barrier is thought to be imposed by the rigid environment thus preventing population of an emitting level which is geometrically distorted with respect to the ground state. In this regard, it is interesting to note the recent result that analysis of the $^4T_{2g} \leftarrow {}^4A_{2g}$ absorption for $Cr(NH_3)_6^{3+}$ in crystals at 4°K shows that bond expansions of 0.12Å must occur in the $^4T_{2g}$ state relative to $^4A_{2g}$.[20] Perhaps the best understood of these diverse phenomena are the fluorescence yield dependences of certain sterically crowded butadienes,[21] stilbenes[22-24] and ethylenes[25] on solvent rigidity. In these cases a decrease in radiationless decay with increasing solvent rigidity is attributed to the quenching of vibrational motion about an essential bond thus preventing geometrical isomerization. We think that there is a strong possibility that geometrical isomerization is also responsible for the rigidity dependent radiationless decay in $M(P{=}P)_2Cl$ complexes. It has long been established that cis → trans isomerization accompanies population of ligand field states in square planar Pt(II) complexes,[26,27] and it seems certain that motion such as square planar → tetrahedral could easily activate radiationless decay. Furthermore, a large molecular displacement would be involved which should be quite sensitive to environmental rigidity. The emission of $Rh(P{=}P)_2Cl$ shows a large Stokes shift which is attributable to distortion in the emitting E_u level. In fact it must be this distortion, rather than the population of an MLCT state, which gives rise to the solvent relaxation effects. This follows because the analogous MLCT state is responsible for the $Ir(P{=}P)_2Cl$ emission, and solvent relaxation effects and the Stokes shift are nearly negligible.

All of the above remarks apply to $Ir(P{=}P)_2Cl$ radiationless decay as well, except that the tendency to isomerization may not be so pronounced as in the $Rh(P{=}P)_2Cl$ case. This could explain the observation that the emission yield decrease occurs more gradually with increasing temperature for the Ir(I) complex and that the midpoint of the τ vs. temperature curves lies approximately 20°K to higher temperature. Finally, the Ir(I) complex differs from the Rh(I) material in that a thermally activated radiationless decay, in addition to the solvent dependent path, also exists. The origin of this observation is unknown at present.

ACKNOWLEDGMENT

It is a pleasure to acknowledge conversations with Drs. A. Lempicki, E. Johnson, B. McCollum, L.S. Forster and M. Wrighton regarding this work. Also, we thank the Air Force Office of Scientific Research for support under contract F49620-77-C-0015.

REFERENCES

1. G.L. Geoffroy, M.S. Wrighton, G.S. Hammond and H.B. Gray, J. Am. Chem. Soc. 96, 3105 (1974).

2. G.L. Geffroy, H. Isci, J. Litrenti and W.R. Mason, Inorg. Chem. 16, 1950 (1977).

3. L.J. Andrews, Inorg. Chem. 17, 3180 (1978).

4. L. Vaska and D.L. Catone, J. Am. Chem. Soc. 88, 5324 (1966).

5. D.W. Davidson and R.H. Cole, J. Chem. Phys. 19, 1484 (1951).

6. F. Perrin, J. Phys. Radium 5, 497 (1934).

7. E. Lippert, Z. Naturforsch 10a, 541 (1955).

8. N. Mataga, Y. Kaifu and M. Koizumi, Bull. Chem. Soc. Japan 28, 690 (1955).

9 W.R. Ware, S.K. Lee, G.J. Brant and P.P. Chow, J. Chem. Phys. 54, 4729 (1971).

10. N.G. Bakhshiev, Y.T. Mazurenko and I.V. Piterskaya, Opt. Spectros. 21, 307 (1966).

11. W. Rapp, H. Klingenberg and H.E. Lessing, Ber. Bunsenges Physik. Chem. 75, 883 (1971).

12. H.E. Lessing and M. Reichert, Chem. Phys. Let. 46, 111 (1977).

13. P. Debye, Polar Molecules (Dover, New York, 1929).

14. F.E. Lytle and D.M. Hercules, J. Am. Chem. Soc. 91, 253 (1969).

15. S.R. Allsopp, A. Cox, T.J. Kemp and W.J. Reed, J.C.S. Faraday II 1275 (1978).

16. M. Wrighton and D.L. Morse, J. Am. Chem. Soc. 96, 998 (1974).

17. W. Targos and L.S. Forster, J. Chem. Phys. 44, 4342 (1966).

18. R.J. Watts and D. Missimer, J. Am. Chem. Soc. 100, 5351 (1978).

19. P.J. Giordano, S.M. Fredericks, M.S. Wrighton and D.L. Morse, J. Am. Chem. Soc. 100, 2257 (1978).

20. R.B. Wilson and E.I. Solomon, Inorg. Chem. 17, 1729 (1978).

21. J. Kordas and M.A. El-Bayoumi, J. Am. Chem. Soc. 96, 3034 (1978).

22. J. Saltiel and J.T. D'Agostino, J. Am. Chem. Soc. 94, 6445 (1972).

23. S. Sharafy and K.A. Muszkat, J. Am. Chem. Soc. 93, 4119 (1971).

24. M. Sumitani, N. Nakashima, K. Yoshihara and S. Nagakura, Chem. Phys. Let. 51, 183 (1977).

25. H.H. Klingenberg, E. Lippert and W. Rapp, Chem. Phys. Let. 18, 417 (1973).

26. P. Haake and T.A. Hylton, J. Am. Chem.Soc. 84, 3774 (1962).

27. V. Balzani and V. Carassiti, J. Phys. Chem. 72, 383 (1968).

Unclassified

REPORT DOCUMENTATION PAGE

READ INSTRUCTIONS BEFORE COMPLETING FORM

1. REPORT NUMBER: AFOSR-TR- 79-0832	2. GOVT ACCESSION NO.
3. RECIPIENT'S CATALOG NUMBER	
4. TITLE (and Subtitle): NEW LASERS BASED ON TRANSITION METAL COMPLEXES.	5. TYPE OF REPORT & PERIOD COVERED: Final 1 Oct 76 - 1 Oct 78
	6. PERFORMING ORG. REPORT NUMBER
7. AUTHOR(s): L. Andrews, E. Johnson, A. Lempicki	8. CONTRACT OR GRANT NUMBER(s): F49620-77-C-0015
9. PERFORMING ORGANIZATION NAME AND ADDRESS: GTE Laboratories, Inc. 40 Sylvan Road Waltham, MA 02154	10. PROGRAM ELEMENT, PROJECT, TASK AREA & WORK UNIT NUMBERS: 61102F 2301/A1
11. CONTROLLING OFFICE NAME AND ADDRESS: AFOSR/NP Bolling AFB Wash DC 20332	12. REPORT DATE: Apr 79
	13. NUMBER OF PAGES: 69
14. MONITORING AGENCY NAME & ADDRESS (if different from Controlling Office): Final rept. 1 Oct 76-1 Oct 78,	15. SECURITY CLASS. (of this report): unclassified
	15a. DECLASSIFICATION/DOWNGRADING SCHEDULE

16. DISTRIBUTION STATEMENT (of this Report)

69 P

Approved for public release; distribution unlimited.

DISTRIBUTION STATEMENT A
Approved for public release; Distribution Unlimited

17. DISTRIBUTION STATEMENT (of the abstract entered in Block 20, if different from Report)

TR-79-740.1

18. SUPPLEMENTARY NOTES

19. KEY WORDS (Continue on reverse side if necessary and identify by block number)

20. ABSTRACT (Continue on reverse side if necessary and identify by block number)

The purpose of this program has been to investigate the possibility that luminescent transition metal complexes (TM complexes) might serve as the basis for a new class of lasers tunable in the visible spectral region. At the beginning of the program, sufficient spectroscopic and photophysical data were available to permit calculation of threshold requirements for these new materials, and they were found to lie well within the range of conventional pump sources. This threshold analysis assumed perforce that losses which are unknown do not

DD FORM 1 JAN 73 1473 EDITION OF 1 NOV 65 IS OBSOLETE

UNCLASSIFIED

406 462

SECURITY CLASSIFICATION OF THIS PAGE (When Data Entered)

exist. Virtually, none of these materials is commercially available, so that a large portion of the first year was devoted to synthesis and purification of complexes which appeared most promising for laser applications. This amounted to five groups of materials; metalloporphyrins; ruthenium (II), iridium (III) and rhenium (I) complexed with nitrogen heterocycles and square planar rhodium (I) and iridium (I) phosphines. Emission spectra and lifetimes were routinely measured and compared with literature data to positively identify all synthesized complexes. All promising complexes were tested with the higher energy pump. In addition, a frequency doubled, Q-switched Nd:glass laser was assembled and used to pump complexes in specially designed low-loss resonators.